PALEOCEANOGRAPHY, VOL. 9, NO. 4, PAGES 619-638, AUGUST 1994

Astronomic timescale for the Pliocene Atlantic $\delta^{18}O$ and dust flux records of Ocean Drilling Program site 659

Ralf Tiedemann
GEOMAR, Forschungszentrum für Marine Geowissenschaften, Universität Kiel, Kiel, Germany

Michael Sarnthein
Geologisch-Paläontologisches Institut, Universität Kiel, Kiel, Germany

Nicholas J. Shackleton
The Godwin Laboratory, University of Cambridge, Cambridge, England

Abstract. High-resolution benthic oxygen isotope and dust flux records from Ocean Drilling Program site 659 have been analyzed to extend the astronomically calibrated isotope timescale for the Atlantic from 2.85 Ma back to 5 Ma. Spectral analysis of the $\delta^{18}O$ record indicates that the 41-kyr period of Earth's orbital obliquity dominates the Pliocene record. This is shown to be true regardless of fundamental changes in the Earth's climate during the Pliocene. However, the cycles of Sahelian aridity fluctuations indicate a shift in spectral character near 3 Ma. From the early Pliocene to 3 Ma, the periodicities were dominantly precessional (19 and 23 kyr) and remained strong until 1.5 Ma. Subsequent to 3 Ma, the variance at the obliquity period (41 kyr) increased. The timescale tuned to precession suggests that the Pliocene was longer than previously estimated by more than 0.5 m.y. The tuned ages for the magnetic boundaries Gauss/Gilbert and Top Cochiti are about 6-8% older than the ages of the conventional timescale. A major phase of Pliocene northern hemisphere ice growth occurred between 3.15 Ma and 2.5 Ma. This was marked by a gradual increase in glacial Atlantic $\delta^{18}O$ values of 1‰ and an increase in amplitude variations by up to 1.5‰, much larger than in the Pacific deepwater record (site 846). The first maxima occured in cold stages G6-96 between 2.7 Ma and 2.45 Ma. Prior to 3 Ma, the isotope record is characterized by predominantly low amplitude fluctuations (< 0.7‰). When obliquity forcing was at its minimum between 4.15 and 3.6 Ma and during the Kaena interval, $\delta^{18}O$ amplitude fluctuations were minimal. From 4.9 to 4.3 Ma, the $\delta^{18}O$ values decreased by about 0.5‰, reaching a long-term minimum at 4.15 Ma, suggesting higher deepwater temperatures or a deglaciation. Deepwater cooling and/or an increase in ice volume is indicated by a series of short-term $\delta^{18}O$ fluctuations between 3.8 and 3.6 Ma.

Introduction

One of the major issues in paleoclimatology during the past two decades has been the discovery that orbitally induced changes in solar radiation strongly affect variations in the oxygen isotope record. This has resulted in the development of an astronomically calibrated isotope timescale for the last 2.85 m.y. [*Imbrie et al.*, 1984; *Martinson et al.*, 1987; *Ruddiman et al.*, 1986, 1989; *Raymo et al.*, 1989; *Shackleton et al.*, 1990; *Hilgen*, 1991]. In a joint effort *Shackleton et al.* [1994a, b] and we ourselves have extended the $\delta^{18}O$ stratigraphy independently for the Pacific and Atlantic sediment records back to 5-6 Ma using the tuning techniques of *Imbrie et al.* [1984] and *Hilgen* [1991]. Our analysis was based on both oxygen isotope and dust flux records from Ocean Drilling Project (ODP) site 659 located on top of the Cape Verde Plateau off northwest Africa (Figure 1).

Paper number 94PA00208.
0883-8305/94/94PA00208$10.00

Fluctuations of the benthic oxygen isotope record are sensitive to northern hemisphere ice sheet variations and to changes in deepwater temperature. *Imbrie and Imbrie* [1980] found these variations lag astronomical forcing of Earth's insolation by 5-8 kyr. Prior to 0.6 Ma and during the Matuyama chron, $\delta^{18}O$ variations were dominated by the 41-kyr rhythm of obliquity [*Ruddiman et al.*, 1986; *Raymo et al.*, 1989]. Over the last 0.6 m.y. the variations were dominated by the 100-kyr eccentricity cycle associated with increased variance at the precession bands [Imbrie et al., 1984, 1992, 1993].

The dust flux record off west Africa monitors the history of continental aridity fluctuations in the South Sahara and Sahel zone [*Tiedemann et al.*, 1989; *Tiedemann*, 1991]. The precipitation in the Sahel region of subtropical northwest Africa is primarily controlled by the interaction of northern monsoonal moisture incursions and squall lines [*Dhonneur and Tourre*, 1981]. At present, squall lines are located between 10° and 15° N and are responsible for the generation and injection of dust into the midtropospheric African easterly jet stream (AEJ). The AEJ is the major dust carrier from northwest Africa [*Sarnthein et al.*, 1981]. Today, site 659 is located below the

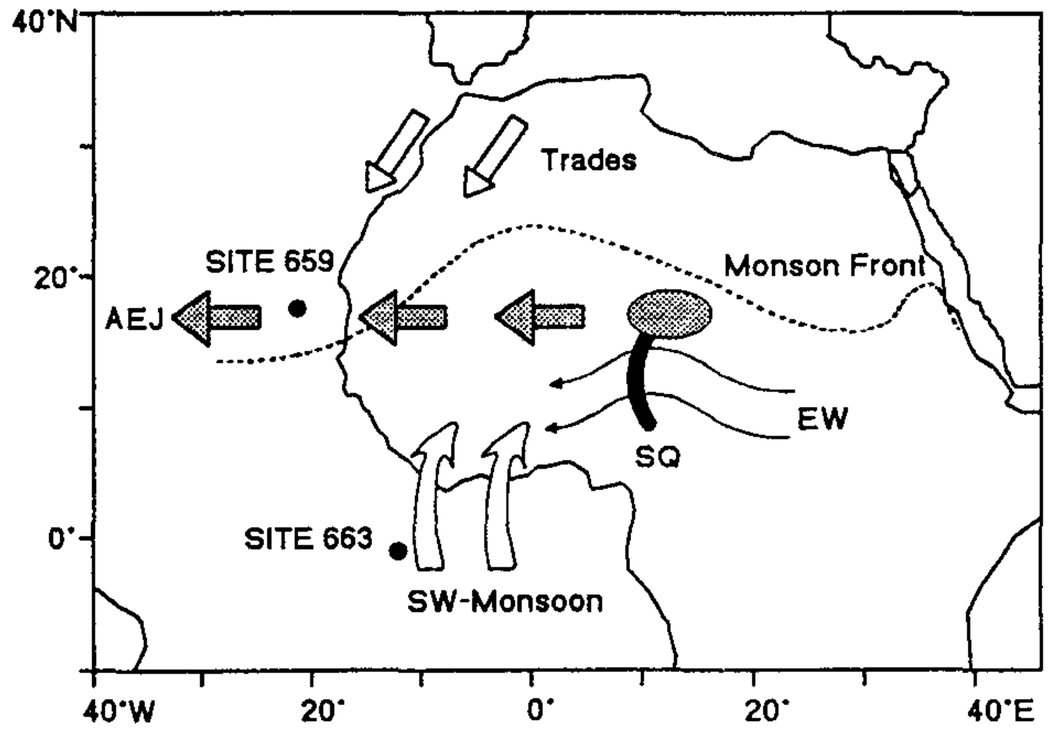

Figure 1. Schematic presentation of the modern meteorological pattern over northwest Africa during northern summer [from *Tetzlaff and Peters*, 1986] and position of site 659 (18°05'N, 21°02'W, 3070 m water depth). The monsoonal transport of water vapor into the Sahel and the formation of rain is based upon a mechanism involving the atmospheric disturbances easterly waves (EW), the squall lines (SQ), and the African easterly jet stream (AEJ) as a product of differential surface heating. All of them organize the rains and the generation and transport of dust. Elliptical shaded area gives the dust cloud related to the squall line.

center of this AEJ dust trajectory [*Tetzlaff and Peters*, 1986]. The modern AEJ dust outbreaks are closely linked to the summer position of the Intertropical Convergence Zone (ITCZ). *Tiedemann et al.* [1989] have shown that the latitudinal position of the AEJ and the ITCZ have remained essentially stationary during the last 4 m.y., and thus did not control changes in Sahelian aridity. Distribution patterns of eolian silt and pollen concentrations for different time slices of the last 18 kyr offshore northwest Africa also suggest a constant summer position of the ITCZ throughout glacial and interglacial times [*Sarnthein et al.*, 1981; *Hooghiemstra et al.*, 1987].

Several paleoclimatic studies have shown that variations in North African aridity parallel changes in high-latitude continental ice volume [e.g., *Parkin and Shackleton, 1973*; *Kolla et al.*, 1979; *Sarnthein et al.*, 1981; *Stein*, 1986] and North Atlantic sea surface temperature [e.g., *Lamb*, 1978; *Palmer*, 1986; *Street-Perrott and Perrott*, 1990], which both vary mainly with 100 kyr and 41 kyr orbital cycles [*deMenocal et al.*, 1993].

South Saharan and Sahelian aridity also responds to precessional low-latitude monsoon forcing [e.g., *Kutzbach*, 1981; *Pokras and Mix*, 1985; *Rossignol-Strick*, 1983]. Based on a magnetic susceptibility record from site 661 (0-3.5 Ma on an untuned timescale), *Bloemendahl and DeMenocal* [1989] reported that fluctuations in Sahelian dust supply underwent a major change in cyclicity between 2.4 and 2.8 Ma. The 41-kyr obliquity cycle was predominant during the last 2.4 m.y., whereas strong precession cycles (23 kyr) dominated prior to 2.8 Ma, that is the interval which is tuned in the present study.

Data Analysis

At site 659, the terrigenous component should largely equate to the siliciclastic sediment fraction, because the South Saharan and Sahelian dust discharge contains less than 4-8% $CaCO_3$ [*Sarnthein et al.*, 1982]. Hence the noncarbonate fraction (100% minus %$CaCO_3$) at this distal site on top of the Cape Verde Plateau (Figure 1) is considered to be purely eolian, because the concentrations of biogenic opal (< 2%), organic carbon (< 0.5%), and volcanic glass are negligible and fluvial sediment supply and turbidites cannot reach this position [*Tiedemann et al.*, 1989]. Actually, the concentration of dust may be slightly higher when considering a few percent of carbonate particles that are neglected in our analyses. By using dust flux rates instead of percentages for the tuning process, we largely exclude effects of percentage dilution.

$CaCO_3$ data from site 659 and the analytical procedures were described by *Tiedemann et al.* [1989] and *Stein et al.* [1989]. Additional measurements were carried out with a LECO analyser. For isotope analysis of the epibenthic foraminifer *Cibicidoides wuellerstorfi*, up to ten specimens were picked from the 250-315μm fraction. The $\delta^{18}O$ values of *C. wuellerstorfi* were adjusted to seawater equilibrium by adding 0.64‰ [*Shackleton and Hall*, 1984] (except for Figure 2). The data set includes isotope data from *Schulz* [1988]. Isotopic analyses were performed using a Finnigan MAT 251 mass spectrometer at the ^{14}C Laboratory of Kiel University using standard methods as described by *Zahn et al.* [1986].

The average sample spacing is 3.5 kyr for the untuned isotope record and 3.0 kyr for the untuned dust flux record. After tuning, the sample spacing increases to 4.3 and 4.0 kyr respectively. For time series analysis the age of each sample was estimated by linear interpolation between the age-depth control points. Then we interpolated each record at constant 3-kyr intervals using a Gaussian weighting method that includes a small amount of prewhitening. After the data had been linearly detrended, we estimated the variance density spectrum and subsequently filtered the data at the dominant frequency bands. Statistical analysis was based on the SPECMAP standard methods [*Jenkins and Watts*, 1968; *Imbrie et al.*, 1984]. For the tuning procedure we used the astronomical solution of *Berger and Loutre* [1991] for the last 5 m.y.

Composite Depth Sections

High-resolution magnetic susceptibility records (2-cm spacing) from three holes (A, B, and C) at site 659 [*Bloemendahl et al.*, 1988] were spliced to obtain a continuous composite record [*Tiedemann*, 1991]. Below 41.05 m, we improved our composite depth model as indicated in Table 1. Core breaks 659A-1/2, -2/3, and -10/11, and 659B-5/6 and -12/13 were not covered with overlapping sections in other cores at site 659 (Figure 2). However, correlation with the $\delta^{18}O$ records from sites 607 and 677 (Figure 3) suggest no significant loss of sediment at core breaks 659A-1/2 (isotope stage 8), 659A-2/3 (isotope stage 15), and 659B-5/6 (isotope stage 59) (Figures 2 and 3). A visual correlation with the isotope curve from the east equatorial Pacific site 846 [*Shackleton et al.*, 1994a] across core break 659A-10/11 suggests that not more than half a 40-kyr cycle of sediment is missed at isotope stage M2. The full recovery across core break 659B-12/13 (stage Gi14) remains uncertain. Results from the tuning itself and the paleomagnetic record discussed below suggest that less than a full precession cycle of sediment thickness is missed. Furthermore, the structure of the

Table 1. New "Pathway" of Composite Depth Levels to Correlate Core Sections in Holes 659A, 659B, and 659C from 41 to 146 m Composite Depth

659A Original Depth, m	659B Original Depth, m	659C Original Depth, m	Composite Depth, m
39.80	(5) 36.00		41.05
41.77	38.73		43.02
42.21	39.19		43.46
44.11	40.60		45.36
(5) 44.40	40.70		45.46
	(5) 43.62		48.38
	(6) 44.67		48.43
(7) 55.30	53.32		57.08
55.40	53.40		57.16
55.50	53.50		57.26
55.60	53.58		57.34
55.68	(6) 53.68		57.44
55.71	53.71		57.47
55.80	53.80		57.56
56.15	(7) 54.10		57.91
56.33	54.20		58.09
56.43	54.30		58.19
56.86	54.40		58.62
57.30	54.73		59.06
57.68	54.93		59.44
57.97	55.23		59.73
58.47	55.77		60.23
58.64	55.93		60.40
58.82	56.10		60.58
59.14	56.43		60.90
59.54	56.78		61.30
59.82	57.08		61.58
60.18	57.44		61.94
60.40	57.68		62.16
61.91	59.16		63.67
62.13	59.37		63.89
63.42	60.62		65.18
64.16	61.30		65.92
64.40	61.51		66.13
(7) 64.65	61.69		66.31
(8) 64.80			66.37
64.95	(7) 63.25		67.87
65.16	63.34		68.08
66.20	(8) 63.60		69.12
66.35	63.69		69.27
66.40	63.80		69.32
66.83	64.20		69.75
67.45	64.88		70.37
67.98	65.41		70.90
68.42	65.90		71.34
68.90	66.40		71.82
69.08	66.63		72.00
69.58	67.10		72.50
69.72	67.28		72.64
70.15	67.69		73.07
70.75	68.32		73.67
71.25	68.80		74.17
72.20	69.77		75.12
(8) 73.02	70.61		75.94
(9) 74.36	71.57		76.90
74.93	(8) 72.55		77.88
75.32	(9) 73.22		78.27
75.90	73.83		78.85
76.50	74.45		79.45
77.05	74.98		80.00
77.79	75.70		80.74
78.68	(9) 76.57		81.63
81.03	(10) 78.59		83.98
81.12	78.68		84.07
81.88	79.48		84.83
(9) 82.31	79.99		85.34
(10) 84.68	82.78		88.13
85.36	83.50		88.81
85.52	83.70		88.97
86.00	84.11		89.45
86.20	84.41		89.65
86.42	84.74		89.87
86.77	85.12		90.22
87.09	85.50		90.54
87.74	86.20		91.19
88.89	(10) 87.50		92.34

Table 1. (continued)

659A Original Depth, m	659B Original Depth, m	659C Original Depth, m	Composite Depth, m
(10) 89.30	(11) 88.70		92.75
(11) 93.70	93.10		97.15
94.88	94.30		98.33
96.26	(11) 95.93		99.71
98.30	(12) 97.97	(5) 100.33	101.75
98.69	98.17	100.80	102.14
98.91	98.50	101.05	102.36
99.18		101.38	102.63
99.33	99.19	101.57	102.78
99.62	99.40	101.90	103.07
99.97	99.71	102.20	103.42
100.10	99.87	102.38	103.55
100.14	100.01	102.39	103.59
100.18	100.03	102.43	103.63
100.43	100.22	102.71	103.88
100.55	100.40	102.85	104.00
(11) 101.09	100.87	103.37	104.54
	101.33	103.82	105.00
	101.88	104.41	105.55
	102.10	104.69	105.77
	102.34	104.90	106.01
	102.50	105.08	106.17
	102.87	105.45	106.54
	103.11	105.70	106.78
	103.30	105.90	106.97
	103.58	106.13	107.25
	103.82	106.42	107.49
	104.19	106.84	107.86
	104.45	107.08	108.12
	104.82	107.48	108.49
	105.09	107.70	108.76
	105.29	107.90	108.96
	105.57	108.21	109.24
	105.74	108.43	109.41
	105.95	108.59	109.62
	(12) 106.17	(5) 108.80	109.84
	(13) 107.95	(6) 109.81	111.62
	108.30	110.18	111.97
	108.52	110.42	112.19
	108.74	110.68	112.41
	109.55	111.49	113.22
	110.05	112.00	113.72
	110.30	112.21	113.97
	110.50	112.46	114.17
	(13) 110.72	112.68	114.39
(13) 112.55		114.39	116.10
113.38		114.93	116.93
113.57		115.13	117.12
114.03		115.30	117.58
114.30		115.62	117.85
114.88		116.01	118.43
115.33		116.25	118.88
115.83		116.67	119.38
116.40		117.08	119.55
116.93		117.41	120.48
117.00		117.48	120.55
118.15		(6) 118.15	121.80
119.30	(14) 116.82		122.85
119.74	117.23		123.29
120.00	117.80		123.55
120.40	118.54		123.95
120.70	118.81		124.25
121.11	119.85		124.66
(13) 121.19	119.92		124.73
(14) 122.40	120.94		125.75
122.67	121.25		126.02
124.00	122.65		127.35
125.73	(14) 124.58		129.08
128.52	(15) 127.89		131.87
128.70	128.09		132.05
128.89	128.37		132.24
129.06	128.58		132.45
129.21	128.70		132.57
129.37	128.90		132.77
(14) 129.74	129.28		133.15
(15) 132.03	131.00		134.87
132.36	131.60		135.47
132.71	131.77		135.64
132.86	131.93		135.80
133.08	132.20		136.07

Table 1. (continued)

659A Original Depth, m	659B Original Depth, m	659C Original Depth, m	Composite Depth, m
133.54	132.98		136.85
133.89	133.30		137.17
134.12	133.68		137.55
134.40	134.00		137.87
134.72	134.45		138.32
135.29 ←	(15) 135.18		139.05
135.61 →	(16) 135.78		139.37
136.56	136.78		140.37
137.43	137.43		141.02
137.58	137.95		141.54
(15) 138.18	138.53		142.12
(16) 141.48	140.00		143.59
141.73 ←	140.30		143.89
142.29	140.98		144.45
143.12	141.57		145.28
143.92	142.10		146.08

Between-hole correlations are based on magnetic susceptibility data [*Bloemendahl et al.*, 1988]. Original depth values have been corrected for voids when occurring within sediment cores (length of sediment core equals total length of sediment core minus length of voids). Core numbers are given in parenthesis.

isotope curve above and below this gap parallels the benthic isotope curve from site 846 [*Shackleton et al.*, 1994a].

Stratigraphy of the Last 2.85 m.y.

Within the orbitally tuned global oxygen isotope record for the last 2.85 Ma, 116 isotope stages were counted [*Imbrie et al.*, 1984; *Martinson et al.*, 1987; *Ruddiman et al.*, 1986, 1989, *Raymo et al.*, 1989] (see Figure 3). For stages 1 to 104 (2.6 Ma), we followed the isotope timescale of *Shackleton et al.* [1990]. This was generated from ODP site 677 using the *Imbrie and Imbrie* [1980] ice volume model as the tuning target. Shackleton's new match between the isotope record and the orbital models for isotope stages 17-19, 21, and 35 resulted in a more linear profile of the sedimentation rates and in older stage ages prior to 620 ka. These ages are older than indicated by the TP607 timescale of *Ruddiman et al.* [1989] and *Raymo et al.* [1989]. This implies that the magnetic reversal ages for the last 3 m.y. are 5-7% older than currently accepted K/Ar-dated magnetic boundaries of *Berggren et al.* [1985]. Evidence for older reversal ages also comes from more

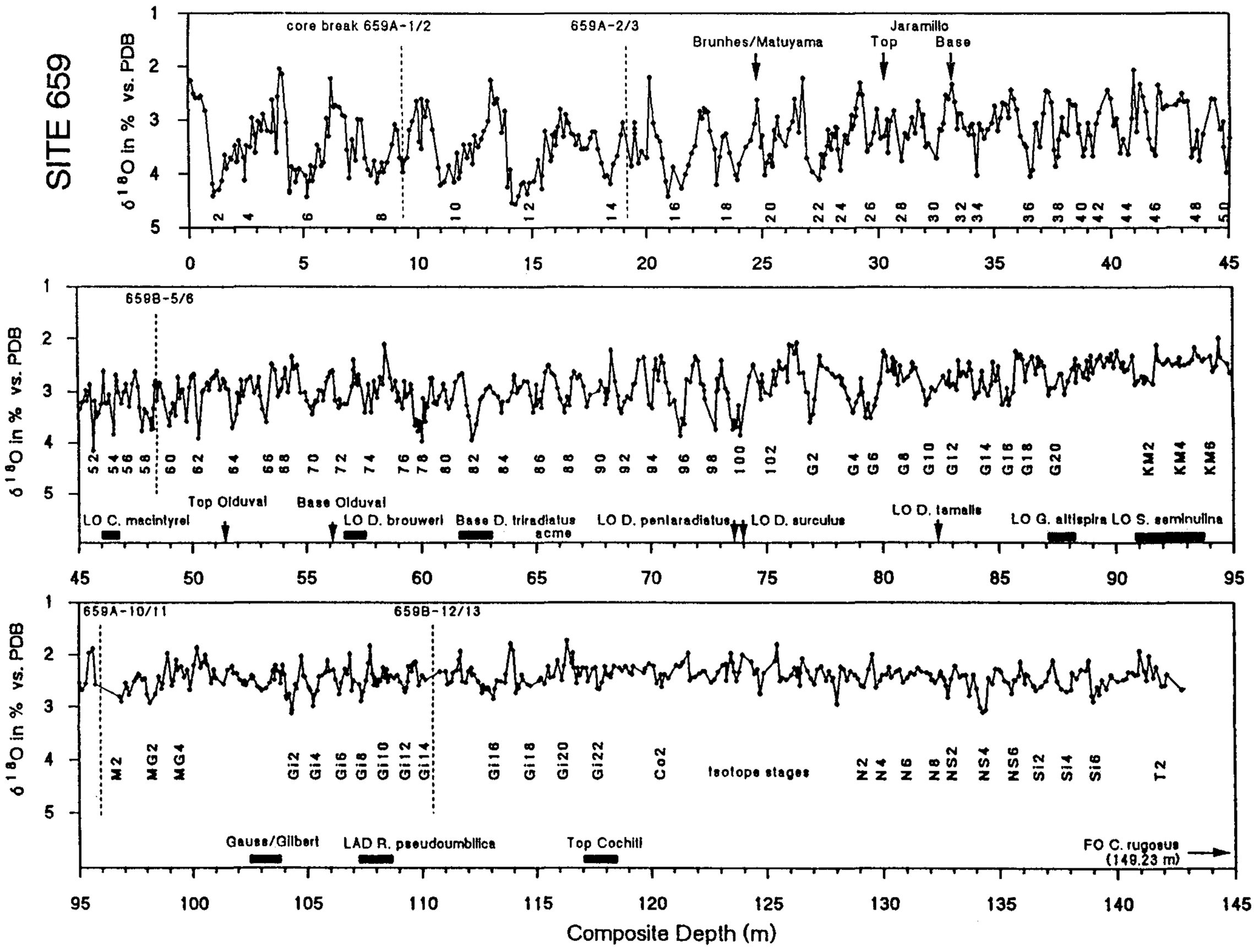

Figure 2. Benthic $\delta^{18}O$ record from site 659 plotted to composite depth. Isotope stage numbers and paleomagnetic and biostratigraphic boundaries [*Ruddiman et al.*, 1988; *Chepstow-Lusty et al.*, 1989] are indicated. Isotope values from *C. wuellerstorfi* are not adjusted to seawater equilibrium. Core breaks with no overlapping sections are indicated by vertical dashed lines.

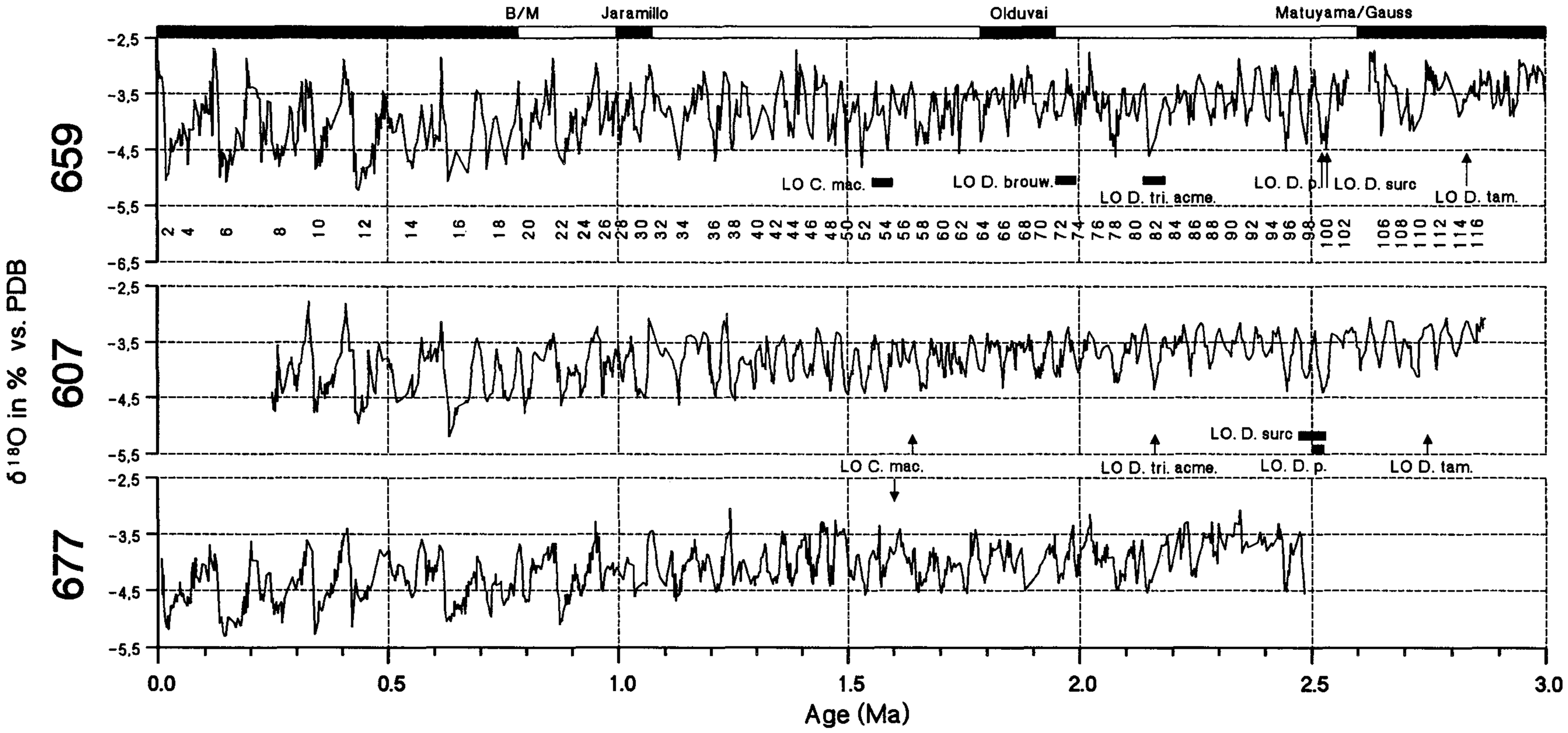

Figure 3. Benthic $\delta^{18}O$ record from site 659 correlated to benthic $\delta^{18}O$ records from North Atlantic site 607 [*Ruddiman et al.*, 1989; *Raymo et al.*, 1989] and Pacific Site 677 [*Shackleton et al.*, 1990]. Records are plotted to site 677 timescale. Isotope stages are labeled. Age ranges of magnetic and biostratigraphic boundaries are plotted for comparison (summarized in Table 2). Abbreviations are mac., *macintyrei*; brouw., *brouweri*; tri. acme, *triradiatus acme*; p., *pentaradiatus*; surc., *surculus*; and tam., *tamalis*.

accurate $^{40}Ar/^{39}Ar$ dating of the Brunhes-Matuyama boundary at 783 ka [*Baksi et al.*, 1992], from the upper Jaramillo boundary at 0.99 Ma [*Tauxe et al.*, 1992], from the base of the Olduvai subchron at 1.98 Ma [*Walter et al.*, 1991] and from the Reunion event at 2.14 Ma [*Baksi et al.*, 1993].

All oxygen isotope stages for the last 2.85 m.y. were identified by visual correlation with the benthic isotope records from site 607 [*Ruddiman et al.*, 1989] and site 677 [*Shackleton et al.*, 1990], except for stage 104 (Matuyama/Gauss boundary) (Figure 3) that is not observed at site 659. This may be due to drilling distortions or to a small hiatus. The magnetic reversal ages obtained for the Brunhes/Matuyama boundary and the Jaramillo and Olduvai chron at site 659 (Table 2) are almost identical to those calculated by *Shackleton et al.* [1990]. At site 659, this timescale produced a good match between the amplitude fluctuations in orbital obliquity and the 41-kyr filter output from the $\delta^{18}O$ record (Figure 4).

Astronomical Calibration of the Timescale (2.85-5 m.y.)

The age of the oxygen isotope and dust flux records were initially interpolated from four control points: (1) isotope stage 116 (2.85 Ma, obtained by adding 120 kyr to the estimates of *Raymo et al.* [1989], according to an age of 2.6 Ma for the Matuyama/Gauss boundary, as suggested by *Shackleton et al.* [1990]), (2) the Gauss/Gilbert boundary (3.4 Ma, *Berggren et al.* [1985]), (3) the Top Cochiti (3.88 Ma, *Berggren et al.* [1985]), and (4) the first occurrence of *C. rugosus* (4.6 Ma, *Backmann and Shackleton* [1983]). These records comprise the untuned Pliocene timescale.

The untuned dust flux frequency spectrum is dominated by a 320-kyr period, implying that the long-term Sahelian aridity variations are related to the 400-kyr eccentricity cycle (Figure 5). This requires that the record be expanded by a factor of 1.25. The result is that the high-frequency peaks between 19 and 15 kyr in the untuned record (Figure 5) record are associated with precessional forcing. The 30-kyr peak in the dust flux and the 32-kyr peak in the untuned isotope spectra are both related to variations in obliquity. Eccentricity forcing is the weakest of the orbital parameters and modulates the strength of precession (e sin w; e is eccentricity and w is longitude of perihelion). The strong eccentricity signal indicates that precessional periods should also be apparent in the dust flux spectrum (Figure 5). We smoothed the dust flux record for the last 2.85 m.y. and found that the eccentricity cycle was weak but still apparent (Figure 6). The dominant peaks in the untuned oxygen isotope spectrum occur at 32 kyr and 86 kyr and may correspond to the obliquity and eccentricity cycles, respectively (Figure 5).

The first step in calibrating the untuned timescale older than 2.85 Ma was to correlate the 320-kyr minima in the dust flux record to the minima of the 400-kyr period of eccentricity (Figure 6). After this preliminary tuning of the record, the mean estimated sedimentation rate for this time interval decreased from 4.5 to 2.9 cm/kyr. This is very close to the rate of 3.0 cm/kyr for the last 2.85 m.y., indicating a nearly constant rate of sediment accumulation over the entire interval. We initially found a very good match in amplitude variations between the orbital precession and dust flux signal. Hence, for establishing a more detailed timescale from 2.85 to 5 Ma, we rely on fine-tuning the dust flux record to precession rather than tuning the $\delta^{18}O$ record to obliquity. There are still more reasons for preferring the dust flux signal. The record of orbital precession is better structured than the obliquity record (Figure 4). The precession signal contains a higher variability in amplitude fluctuations versus time. The record of orbital obliquity is characterized by very low and uniform amplitudes over long intervals, especially from 3.0 to 3.5 Ma and from 4.0 to 4.5 Ma. On average, the amplitudes of the orbital obliquity and the $\delta^{18}O$ record are 1/3 lower between 3.0 and 4.5 Ma than during the late Pliocene. As a result, there are some intervals over which the signal-to-noise ratio of the $\delta^{18}O$ record is so low that tuning to obliquity would lack sufficient precision. In contrast, the dust flux signal remains strong during the last 5 m.y.

Before tuning the dust flux record older than 2.85 Ma to precession, we determined the phase relationship between the dust flux and the insolation record for the subsequent time interval, from 2.0 to 2.6 Ma. Cross-spectral analysis between the dust flux and northern hemisphere July insolation (65°N) showed significant coherence (k = 0.95) over the precession band, and dust flux maxima slightly lagged insolation minima by 14°±8° (1 kyr). This implies that dust flux maxima corresponded to minimum northern hemisphere summer insolation levels (at the precession band) associated with weak summer monsoons that resulted in less vegetation in the South Sahara and Sahel zone. This result agrees with modeling studies [*Kutzbach*, 1981; *Prell and Kutzbach*, 1987] and with paleoclimatic evidence from the Saharan and Indian subcontinent [*Street and Grove*, 1979; *Rossignol-Strick*, 1983; *Kutzbach and Street-Perrott*, 1985; *Pokras and Mix*, 1985]. We fine-tuned the dust flux maxima directly to summer insolation minima (July), assuming no phase differences (Figure 4). Assuming zero phase differences for the early and middle Pliocene might be an oversimplification of the true phase relationship, but small phase differences would only result in a minor error of the tuned timescale.

We used four independent methods to test our correlation between the insolation and dust flux records: (1) Tuning of precession resulted in a concentration of variance over all the main orbital frequencies (Figure 5). The precession component of the dust flux accounts for about 30% of the total variance and is highly coherent (k = 0.97) with the 65°N July insolation record, as indicated by cross-spectral analysis (Figure 5). Significant coherence of about 0.71 also occurs with the obliquity component. The strong concentration of power at the eccentricity periods (400 kyr and 100 kyr) may indicate that the subtropical northwest African climate was sensitive to the eccentricity modulation of the precessional component of insolation. The precession and eccentricity peaks in the dust flux spectrum account for 67% of the total variance. The dominant period of the $\delta^{18}O$ record was attributable to obliquity (41 kyr), but significant variance also existed at the precessional band and 100 kyr eccentricity period (Figure 4). Significant coherence with northern hemisphere summer insolation occurred at the obliquity (k =

Table 2. Comparison of Conventional and Astronomically Calibrated Magnetostratigraphic and Biostratigraphic Age Control Points and Their Correlation to the Oxygen Isotope Nomenclature

Magnetic Reversals and Biostratigraphic Datums	Site 659 Composite Depth, m	Isotope Stage			Age, Ma	Astronomically Calibrated Ages, Ma			Age, Ma
		This Work	*Raymo et al.* [1989]	*Shackleton et al.* [1990]	*Berggren et al.* [1985]	This work	*Shackleton et al.* [1990, 1994b]	*Hilgen* [1991b]	*Cande and Kent* [1992]
Brunhes/ Matuyama	24.80	19	19	19	0.73	0.78	0.78		
Top Jaramillo	30.52	27	27	27	0.92	0.99	0.99		
Base Jaramillo	33.20	31	31	31	0.98	1.07	1.07		
Top Olduvai	51.56	63	63/64	63	1.66	1.78	1.77	1.79	
Base Olduvai	56.16	71	72	71	1.88	1.94	1.95	1.95	
Gauss/Gilbert	102.47 - 103.87				3.40	3.59 ± 0.03	3.59	3.58	3.55
Top Cochity	117.00 - 119.18				3.88	4.17 ± 0.03	4.20	4.18	4.03
LO C. macintyrei	46.02 - 46.68	53 - 55	57	55	1.45 (2)*	1.58 ± 0.02	1.60		
LO D. brouweri	56.37 - 57.66	72 - 73	71 - 72		1.87 (1)*	1.97 ± 0.02			
Base D. triradiatus acme	61.56 - 63.06	81 - 83	82		2.07 (2)*	2.16 ± 0.03			
LO D. pentaradiatus	73.52 - 73.72	100 (late)	99/100		2.30 (1)*	2.52			
LO D. surculus	73.82 - 74.02	100 (early)	97 - 100		2.42 (1)*	2.53			
LO D. tamalis	82.35	G10/G11	G7		2.66 (1)*	2.83			
LO G. altispira	87.09 - 88.25	G20			2.94 (1)*	3.02 ± 0.02			
LO S. seminulina	90.95 - 94.95	KM2 - KM6			3.07 (1)*	3.20 ± 0.07			
LO R. pseudoumbilica	107.27 - 108.77	Gi8 - Gi12			3.56 (2)*	3.80 ± 0.04			
FO C. rugosus	148.87 - 149.59				4.60 (2)*	5.23 ± 0.01			

Depth ranges within which magnetic and biostratigraphic boundaries occur at site 659 are taken from *Chepstow-Lusty et al.* [1989], *Weaver et al.* [1989], and K. Baumann and P. Cepek (personal communication, 1993).

*Biostratigraphic datums are indicated by (1) *Hills and Thierstein* [1989] and (2) *Backmann and Shackleton* [1983].

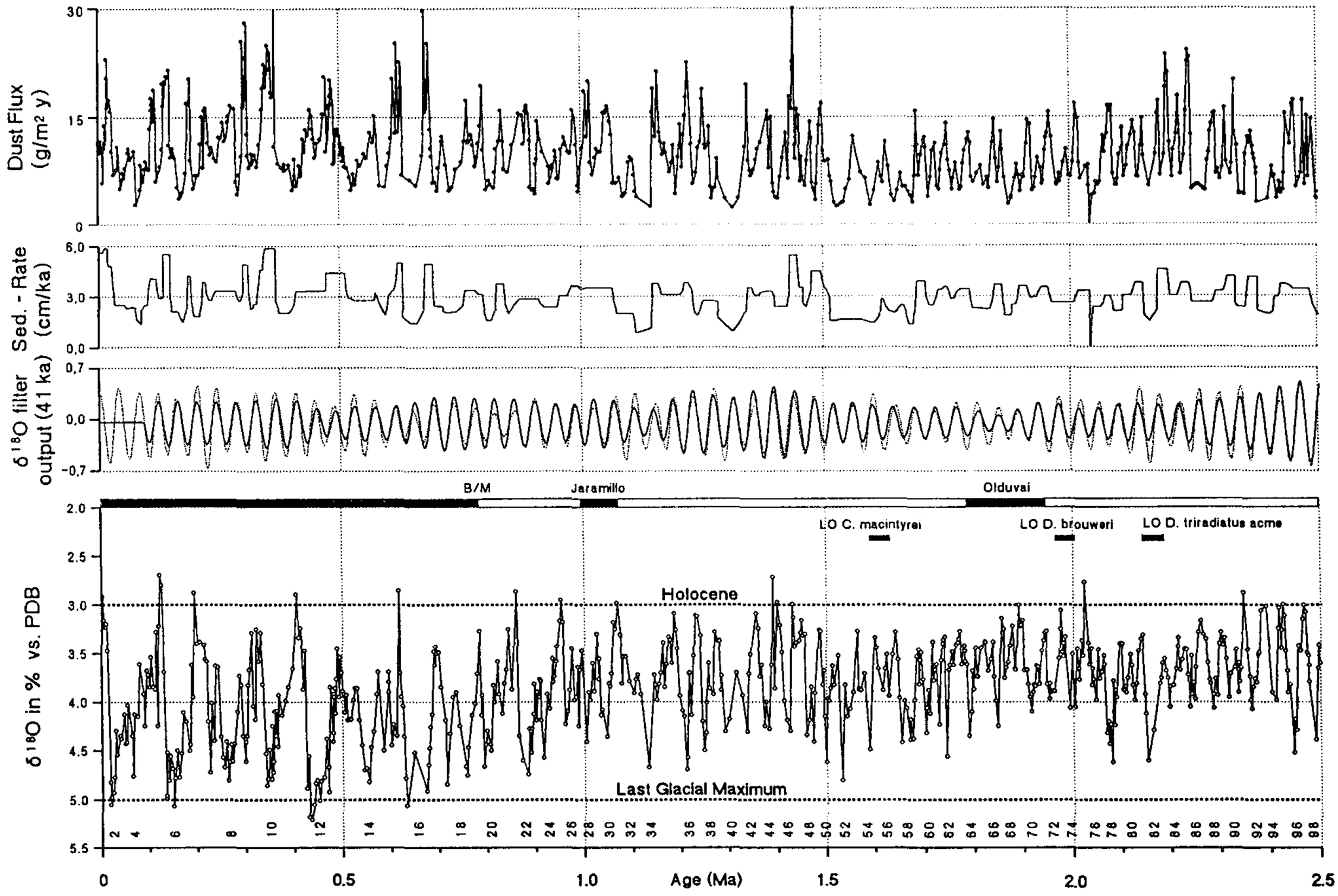

Figure 4. Summary of site 659 records over the last 5 m.y. (a = 0-2.5 m.y. and b = 2.5-5 m.y.): dust flux, sedimentation rate, benthic $\delta^{18}O$ record and its 41-kyr filter (solid) overlain on orbital obliquity (lagged by 8 kyr) (dashed line). The filter used has a central frequency of 0.024 c/kyr and a bandwidth of 0.022 c/kyr. Stratigraphy of the last 2.85 m.y. is based on the site 677 timescale [*Shackleton et al.*, 1990] (Fig. 3). Records from 2.85 to 5 m.y. are plotted to the new timescale, based on tuning the precessional component of the dust flux record to 65°N July insolation [*Berger and Loutre*, 1991]. Isotope stages and magnetic and biostratigraphic boundaries are indicated (see Table 2). Magnetic reversal boundaries for Matuyama/Gauss, Kaena, Mammoth, Base Cochiti, Nunivak, Sidujfall, and Thvera are not documented at site 659 and are transferred from the SCHPS93 timescale [*Shackleton et al.*, 1994b].

0.77) and precession (k = 0.79) frequencies (Figure 5). (2) After tuning the record, we calculated sedimentation rates between the control points for this interval, where fluctuations in sedimentation rates should not be larger than during the last 2.85 m.y. This is reasonable because variations in climate, responsible for fluctuations in eolian sedimentation rates at site 659, were less extreme during the "warm" Pliocene than during the northern hemisphere ice ages. The only other component which influenced the sedimentation rates is $CaCO_3$, because amounts of other sediment components are neglectable. The average carbonate concentration was 70% from 5 to 3 Ma and decreased to 60% during the last 3 m.y. [*Tiedemann*, 1991]. At the shallow position of site 659 at 3080 m water depth, long-term changes in carbonate preservation associated with variations in the depth of the lysocline (today at 4800 m) can be largely excluded [*Curry and Lohmann*, 1985]. However, a 10% decrease in carbonate production is too low to produce a significant decrease in the sedimentation rates. On the other hand, an increased supply of dust during the last 3 m.y. seems more likely to decrease (dilute) the carbonate percentages. From this, we would expect slightly higher sedimentation rates for the last 3 m.y. than before, and not vice versa. During the last 2.85 m.y., sedimentation rates at site 659 varied between 0.9 and 5.9 cm/kyr with a mean value of 3 cm/kyr and a standard deviation of ±1.1 (Figure 4). The changes in sedimentation rates for the new timescale were found to vary between 1 and 5 cm/kyr with a mean value of 2.9 cm/kyr and a standard deviation of ±0.8. (3) Tuning the dust flux record to precession did not affect the dominant response of the isotope record to orbital obliquity forcing. (4) Finally, we can isolate the precession component from the dust flux record by filtering and comparing it to changes in orbital precession. The new timescale from 2.85 to 5 Ma and the interval from 1.6 to 2.85 Ma, using the ages from *Shackleton et al.* [1990] were characterized by a remarkable similarity between the amplitude

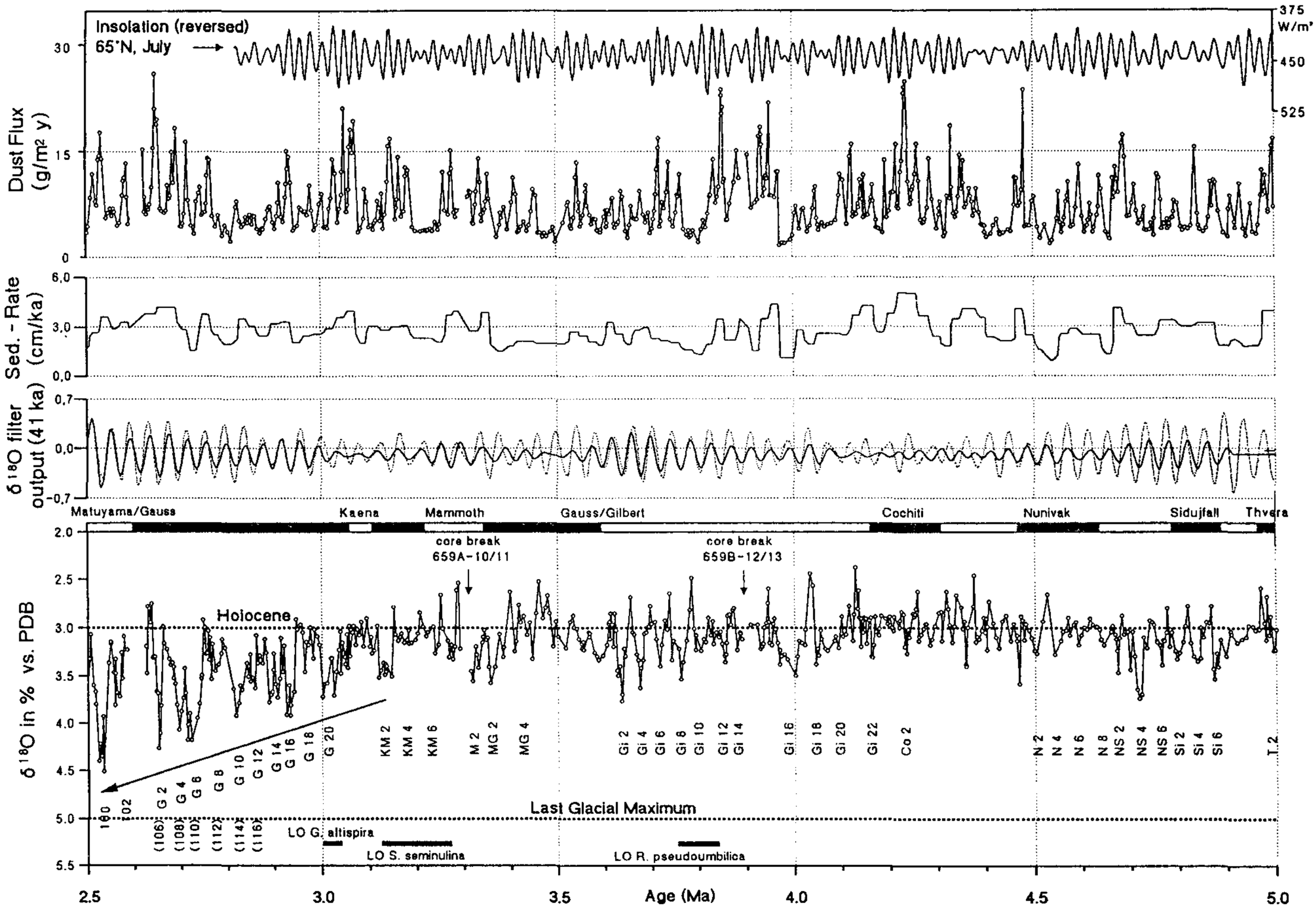

Figure 4. (continued)

variations in orbital precession and the 22 kyr filter output from the dust flux record (Figure 7). This implies that we correctly mapped the climate signal onto the orbital record. Further, it strengthens the conclusion of *Shackleton et al.* [1990] that isotope stages 62-116 are about 120 kyr older than indicated by *Raymo et al.* [1989].

Tuning the time interval 3.7-4 Ma, including core break 659B-12/13, was difficult. This time interval is characterized by three sets of strong precessional amplitude fluctuations in the dust flux and insolation records. Based on the new timescale (Figure 4), the age of the core break 659B-12/13 is about 3.9 Ma. We estimate that 15 kyr of sediment is missing across this core break. Alternatively, we could have moved the first three precessional cycles above the core break by making it one cycle more recent. However, this would result in an antiphase relationship between orbital obliquity and the 41 kyr $\delta^{18}O$ cycles (Figure 4).

Comparing the variations in orbital obliquity with the 41-kyr component filtered from the $\delta^{18}O$ record indicates a mismatch between 4.1 and 4.4 Ma (Figure 4). However, any improvements in the $\delta^{18}O$ correlation to the 41-kyr tilt cycle would be at the expense of the dust flux correlation.

The new timescale from 2.85 to 5 Ma provides revised ages for magnetic and biostratigraphic boundaries (Table 2). *Shackleton et al.* [1994b] and *Hilgen* [1991] both used precession rather than obliquity to calibrate their proxy records. *Hilgen* [1991] correlated a marine record of $CaCO_3$ cycles from Sicily to the astronomical record, and *Shackleton et al.* [1994b] based their tuning on Gamma Ray Attenuation Porosity Evaluation (GRAPE) density records from leg 138 sites. At site 659, the magnetic reversal ages derived for the Gauss/Gilbert boundary (3.59 $\pm$ 0.03 Ma) and Top Cochiti (4.17 $\pm$ 0.03 Ma) are almost identical to those found by *Shackleton et al.* [1994b] and *Hilgen* [1991]. These boundaries occur within the same oxygen isotope stages at both sites 659 and 846. The results of tuning the three independent data sets all agree, and we can conclude that the conventional age estimates for the Pliocene and Pleistocene magnetic boundaries are too young by 5-7%. This was previously pointed out by *Hilgen* [1991]. The revised geomagnetic polarity timescale of *Cande and Kent* [1992] predicts an age for the Gauss/Gilbert boundary and Top Cochiti which is only 1-3% younger than the tuned ages (Table 2). Their age calibration was based on a cubic spline interpolation with controls at the Matuyama/Gauss boundary (2.6 Ma) [*Shackleton et al.*, 1990] and chron C5Bn (14.8 Ma) of the seafloor anomaly sequence.

Nomenclature of Pliocene Isotope Stages

We started a new numbering scheme for the isotope stages below the Matuyama/Gauss boundary at 2.6 Ma (Figures 2, 4b and 8). Capital letters in front of the isotope stage numbers in Figure 8 identify the magnetic polarity interval. Even numbers indicate cold stages and odd numbers indicate warm stages. For

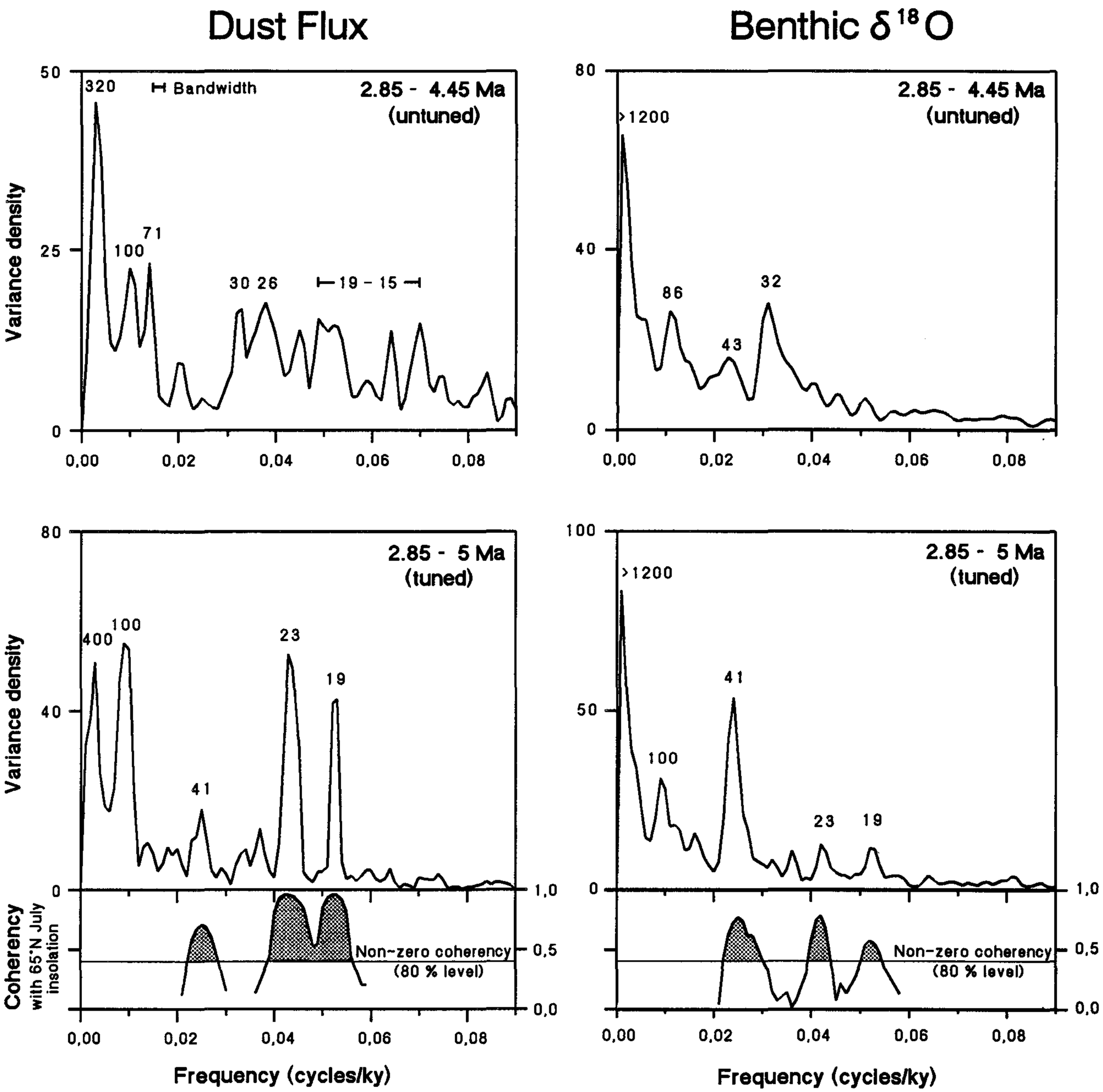

Figure 5. Tuned and untuned $\delta^{18}O$ and dust flux frequency spectra from site 659 for 2.85-5 Ma. Numbers label significant cycles (in kiloyears) at the 80% confidence interval. Spectral analyses was based on Blackman-Tukey technique (3 kyr steps, n = 717, 1/3 lag, bandwidth = 0.002 kyr). Shaded areas indicate significant coherency with 65°N July insolation record above the 80% confidence level (n = 717; number of lags = 100). Isotope cycles > 1.2 m.y. are considered to be artefacts, because the time series is too short to figure out such low frequencies.

example, the first cold stage of the Gauss chron is called G2, and the first cold stage occurring in the magnetic interval between the Kaena and Mammoth is called KM2 (Figure 4). This scheme is discussed further by *Shackleton et al.* [1994a]. For the $\delta^{18}O$ record from site 659 we numbered only stages which have been clearly identified by visual graphic correlation to the Pacific $\delta^{18}O$ record from site 846 [*Shackleton et al.*, 1994a]. Thus these stages are expected to occur as global events (Figure 8).

Oxygen Isotopes

The benthic $\delta^{18}O$ record from site 659 provides a detailed documentation of the timing and magnitude of Pleistocene and Pliocene climate variability in the time and frequency domain. The evolutionary spectra for the last 5 m.y. show the well-known transition from the dominant 41-kyr obliquity period prior to 0.6-1 Ma to the dominant 100-kyr period since that time (Figure 9). The Pliocene dominance of the obliquity

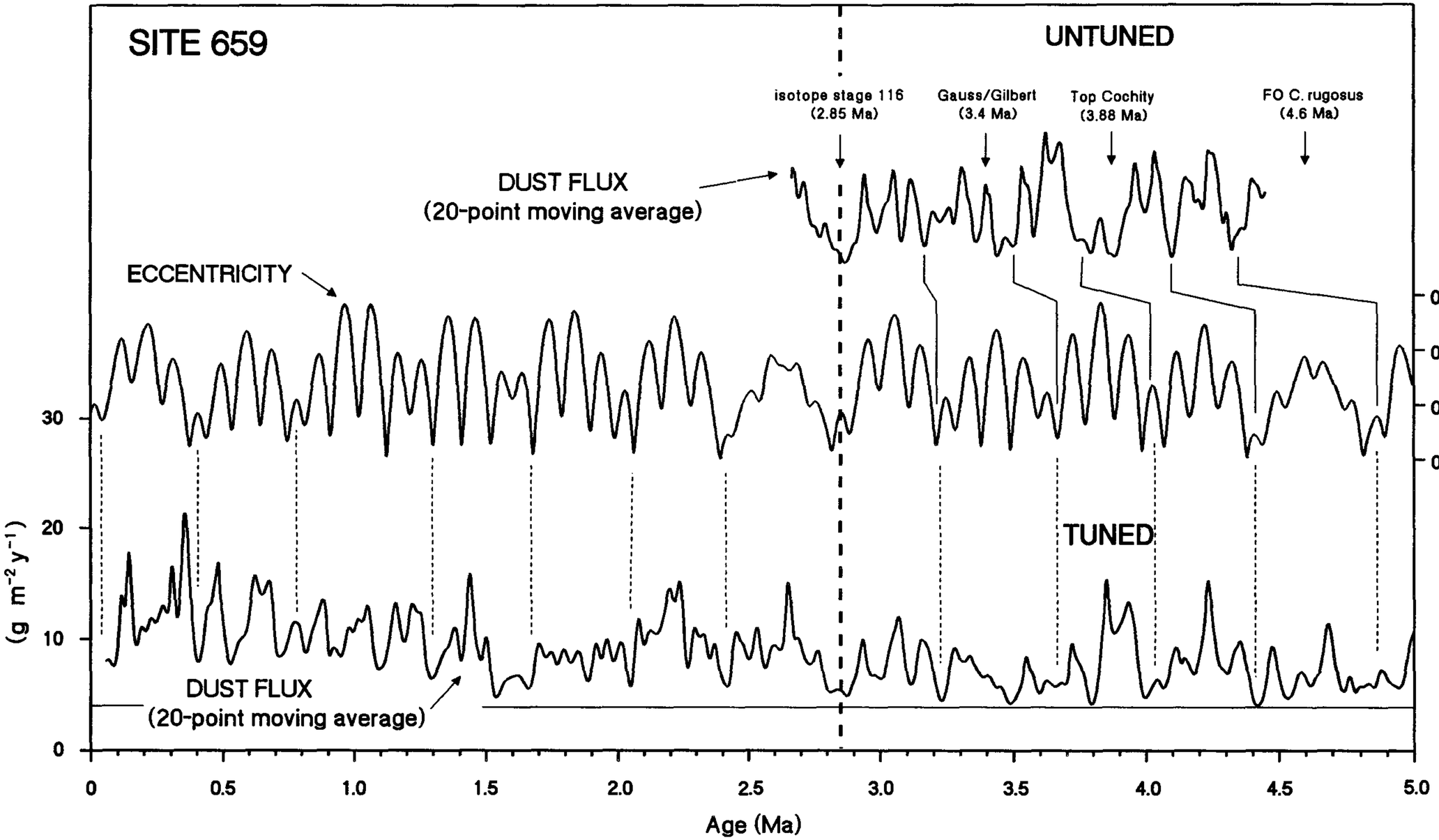

Figure 6. Correlation of large scale dust flux minima to orbital eccentricity minima over the last 5 m.y. A 20-point moving average was used to reduce small-scale variations in the dust flux record connected with precession and obliquity cycles. Age control for the last 2.85 m.y. is based on the timescale from *Shackleton et al.* [1990]. Initial time control of the untuned dust flux record from 2.85 to 4.45 Ma was based on conventional ages for the magnetic and biostratigraphic boundaries Gauss/Gilbert, Top Cochiti, and the first occurence of *C. rugosus* (as indicated on top of the figure). A first astrochronologic calibration of the untuned dust flux record was established by using the correlation points assigned (vertical dashed lines).

period was interrupted by two time intervals of low variance at all orbital frequencies (3-3.5 Ma and 4-4.5 Ma) (Figure 4), coinciding with periods of weak obliquity forcing [*Berger and Loutre*, 1991]. A low but significant response to orbital precession forcing occurred from 0 to 1 Ma, 1.5 to 2.5 Ma, and from 3 to 4.5 Ma.

Long- and short-term variations in the isotope record during the last 2.5 m.y. are similar to those described by *Ruddiman et al.* [1989] and *Raymo et al.* [1989]. However, the amplitude of $\delta^{18}O$ fluctuations at site 659 exceeds those at sites 607 and 677 by about 0.4‰ (Figure 3). This implies larger fluctuations in deepwater temperature/salinity at site 659. The benthic oxygen isotope values prior to 3 Ma varied between 2.5 and 3.5‰ and exhibit low amplitude fluctuations (< 0.7‰) (Figure 4). Extremely low amplitude fluctuations occured from 4.35 to 4.15 Ma and during the Kaena chron, when obliquity forcing was at its minimum (Figure 4). Prior to about 3.2 Ma, peak warm stages were lighter by about 0.2-0.7‰ than the late Holocene value of about 3.0‰. This implies that deepwater was warmer than today or that the global ice volume decreased.

Several long-term trends in isotope variability are observed from 5 to 2.5 Ma (Figure 4). A long-term increase in $\delta^{18}O$ from 5.0 to 4.72 Ma culminates in isotope stage NS4, indicating a deepwater cooling or slight increase in global ice volume. From about 4.7 to 4.3 Ma, a long-term decrease of about 0.5‰ suggests a deepwater temperature increase or deglaciation. The $\delta^{18}O$ values remained low until 4.15 Ma. Deepwater cooling or ice volume increase are indicated by a series of short-term fluctuations with amplitudes of up to 1.2‰ since 4.15 Ma. These are centered between 3.8 and 3.6 Ma at isotope stages Gi2-Gi8. These large amplitudes are paralleled by large-amplitude variations in orbital obliquity. The $\delta^{18}O$ values decreased from 3.6 to 3.45 Ma, followed by a strong increase of 0.7‰ ending at stage M2 (3.3 Ma). The major phase of Pliocene northern hemisphere ice growth occurred about 150 kyr later, between 3.15 Ma (stage KM 2) and 2.5 Ma (stage 100). This is indicated by a gradual increase in the $\delta^{18}O$ maxima of 1‰ to reach a middle Pleistocene level of 4.5‰ (Figure 4). Parallel $\delta^{18}O$ amplitude variations increase up to 1.5‰. This supports the results of several paleoclimate studies identifying this interval as a major episode where large-scale ice rafting occurred in the North Atlantic [e.g., *Shackleton and Hall*, 1984; *Jansen and Sjøholm*, 1991] and North Pacific [e.g., Rea and Leg 145 Scientific Shipboard Party, 1993].

Major insights into the evolution of deepwater circulation during the Pliocene may be deduced from analyzing similarities and differences between the Atlantic record at site 659 and that of the equatorial Pacific site 846 (Figure 8). The cyclicities of both $\delta^{18}O$ records are highly coherent and, on average, in phase at the major orbital frequency bands (Figure 10), although the timescales of the sediment records at sites 846 and 659 were generated by tuning independent data sets (GRAPE density and dust flux). However, the $\delta^{18}O$ amplitude fluctuations at sites 659 and 846 are different. Generally, the amplitudes of isotopic fluctuations appear larger in the Atlantic, despite a partly lower sampling resolution and the slightly lower sedimentation rates at site 659 (averages of 3 versus 4 cm/kyr). For example, glacial-style oscillations of 1‰ characterize the late Gilbert in the Atlantic as compared to amplitudes of 0.7‰ in the Pacific. The same difference applies to the post-Mammoth cooling trend, which is far more

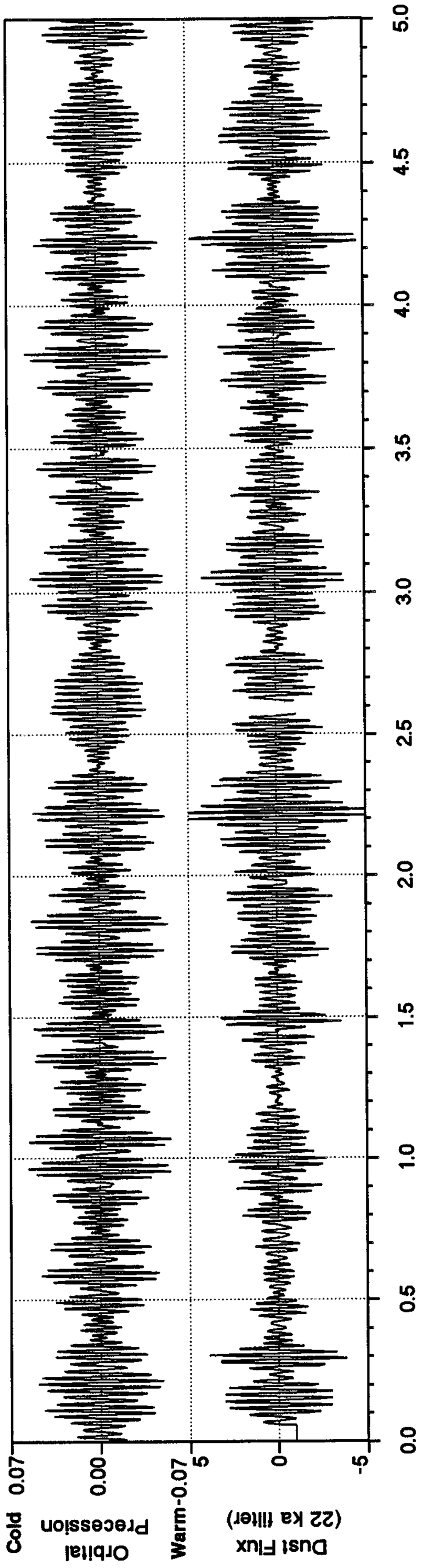

Figure 7. Site 659 dust flux record (Figure 4) filtered at the precession band (central frequency is 0.045 c/ka and bandwidth is 0.036 c/kyr) and compared with orbital precession over the last 5 m.y.

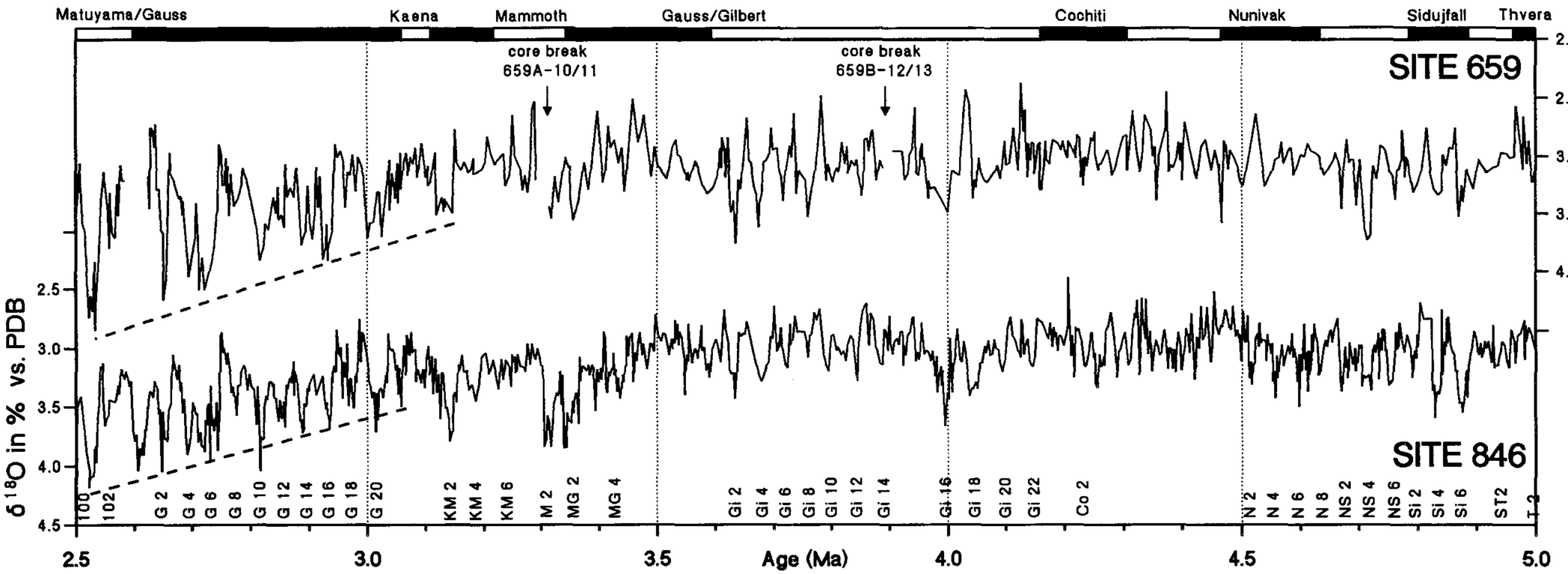

Figure 8. Comparison of the benthic $\delta^{18}O$ records from Atlantic site 659 and Pacific site 846 [*Shackleton et al.*, 1994a]. Records are plotted to their independently tuned timescales. Isotope stages are labeled. Magnetic reversal boundaries for Matuyama/Gauss, Kaena, Mammoth, Base Cochiti, Nunivak, Sidujfall, and Thvera are not documented at site 659 and are transferred from the SCHPS93 timescale [*Shackleton et al.*, 1994b].

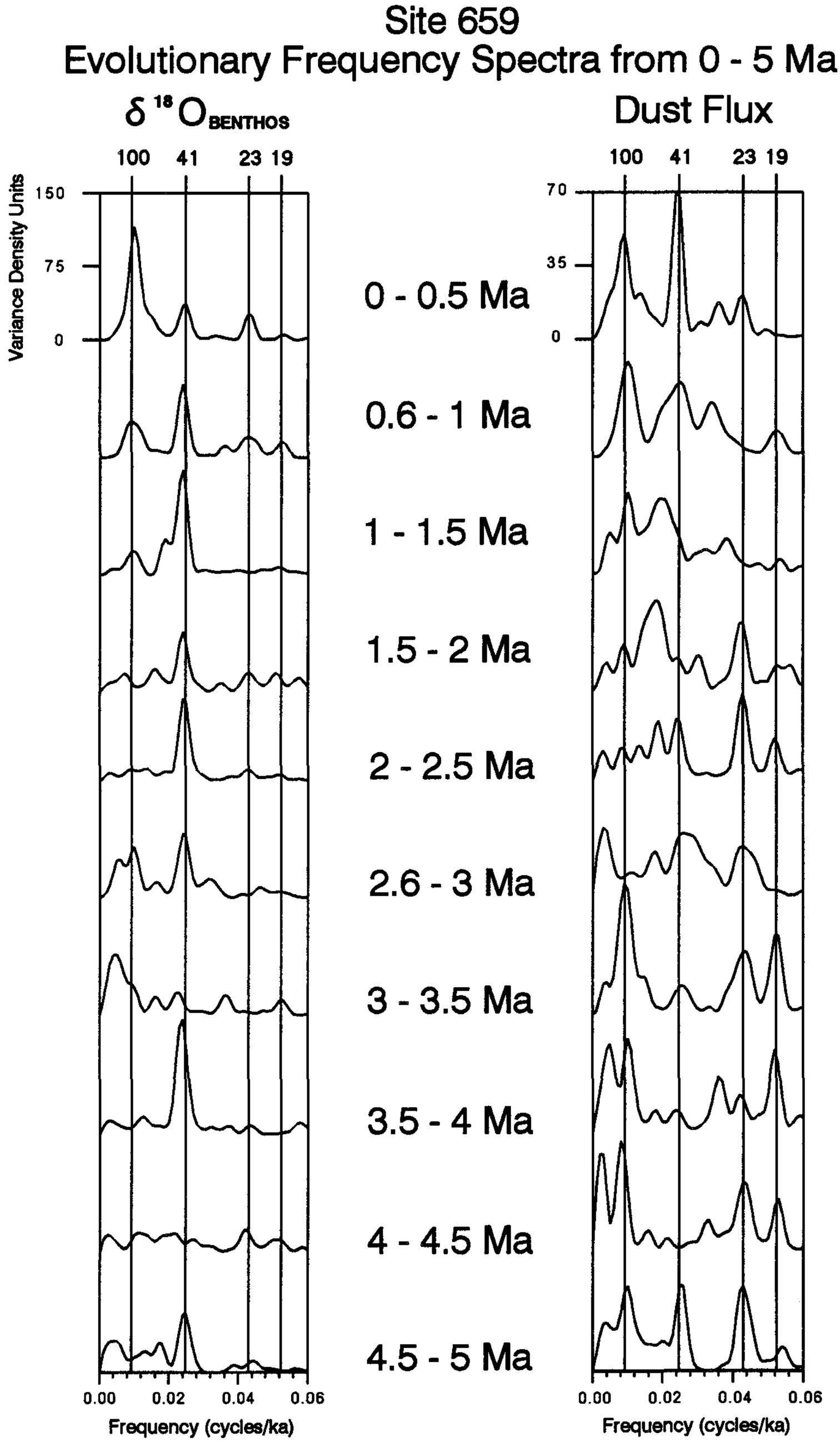

Figure 9. Evolutionary frequency spectra for site 659 $\delta^{18}O$ and dust flux records from 0 to 5 Ma. Each successive spectrum represents an offset of 500 kyr. Spectra were generated using 3-kyr time steps, 1/3 lag, and a bandwidth of 0.004 c/kyr.

pronounced in the Atlantic section (additional increase of cool stages by 0.5‰ from 3.15 to 2.5 m.y.). We surmise that the difference between the Atlantic and Pacific records may be related to a growing admixture of southern source deep water to the position of ODP site 659 at 3000 m water depth during the glacial-style regimes subsequent to the middle Pliocene regime of purely northern-source deepwater advection. This concept is supported by ongoing high $\delta^{13}C$ values from about 4.0-3.1 Ma and an ever-increasing number of $\delta^{13}C$ minima with enlarged amplitudes after this time [*Tiedemann*, 1991].

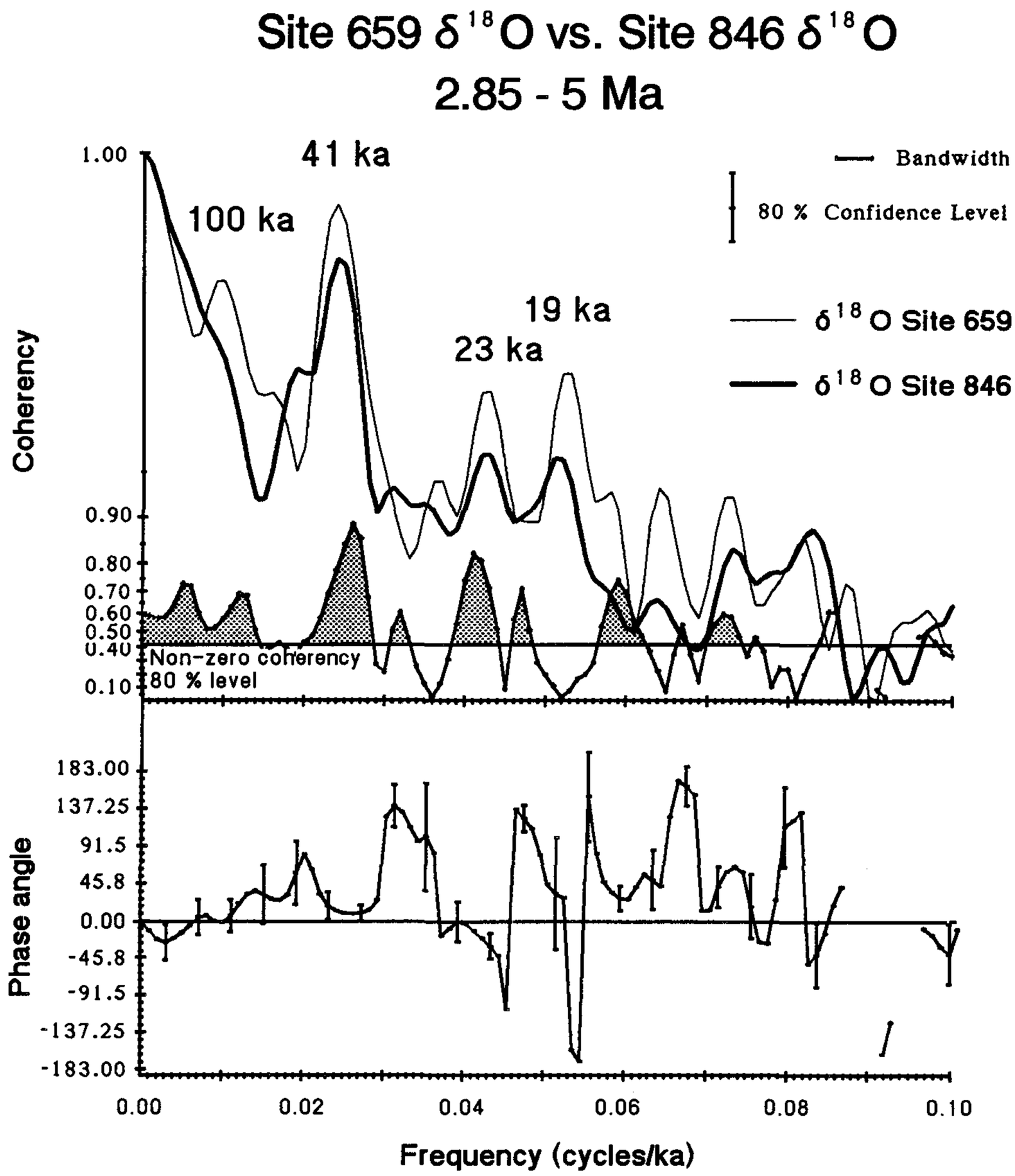

Figure 10. (top) Spectral density and cross coherency for the benthic $\delta^{18}O$ records from Atlantic site 659 and Pacific site 846 over the time interval 2.85-5 Ma (n is 717, time step is 3 kyr, and 100 lags). Significant coherence above the 80% confidence level is demonstrated by shaded areas. (bottom) Phase angle versus frequency plot. Note that both records are in phase at the eccentricity (100 kyr), obliquity (41 kyr) and precession (23 kyr) bands.

Dust Flux

The dust flux record at site 659 reveals that strong arid climate cycles in the South Sahara and Sahel zone persisted throughout the last 5 m.y. (Figure 4). Thus strong Sahelian aridity/humidity cycles started at least 2 m.y. earlier than was previously assumed [*Stein*, 1986]. The long-term evolution of Sahelian aridity has responded primarily to long-term variations in northern hemisphere polar ice volume (Figure 4). The first long-term increase in the dust flux rates occurred from 2.8 to 2 Ma, parallel to the major phase of northern hemisphere ice growth (Figures 4 and 6). There was a subsequent decrease in dust flux from 2 to 1.5 Ma, corresponding to low-amplitude fluctuations in the orbital obliquity and the filtered component of the corresponding $\delta^{18}O$ signal. After the second long-term increase in Sahelian aridity at 1.6-1.4 Ma, the average dust flux rates reached their highest level during the last 1 m.y. This is paralleled by the amplification of the Pleistocene ice age cycles (Figure 4). For the last 2.8 m.y., we estimated that the total duration of arid time intervals with dust flux rates larger than 11 g/(m^2 y) (equal to the late Holocene value) was increased by a factor of 3.5 in comparison to the earlier Pliocene from 2.8 to 5 Ma. Our interpretation of the climatic evolution of the south Sahara and Sahel zone during the last 3 m.y. is very similar to that summarized by *Ruddiman et al.* [1989] for northwest Africa.

We observed no gradual long-term increase in south Saharan-Sahelian aridity and no increase in the amplitude of dust flux variations over the last 5 m.y. (Figure 4) that could be attributed to the impact of Tibetan uplift [*Ruddiman et al.*, 1989; *Ruddiman and Kutzbach*, 1990]. There are two ways to interpret this result: (1) Pliocene Tibetan uplift did not affect the climatic evolution of the S-Sahara and Sahel zone, or (2)

the Tibetan Plateau reached its maximum elevation several million years earlier during the late Miocene at about 7-8 Ma as recently indicated by thermochronologic results from *Harrison et al.* [1992], and not during the Pliocene as predicted by paleobotany studies [*Mercier et al.*, 1987]. Further evidence for a late Miocene uplift associated with enhanced Asian monsoons comes from *Quade et al.* [1989]. They interpret a major shift in the carbon and oxygen isotope records from a pedogenic sediment profile in Pakistan to reflect a strong intensification of the monsoon at about 7.4 Ma.

The short-term frequency response of the Saharan air layer (SAL) dust flux over the last 5 m.y. is summarized in Figure 9. Strong precessional periods and the 100-kyr eccentricity period dominate the dust flux spectrum prior to the major phase of northern hemisphere ice growth from 3 to 5 Ma. However, the obliquity cycle was strong from 4.5 to 5 Ma. From 3 Ma to the present the dust flux response to orbital obliquity increased (at periods of 41 and 54 kyr) and the precession cycles remained strong until 1.5 Ma. During the last 1 m.y. the dust flux record has been dominated by the 100- and 41-kyr cycles. Because the dust flux record did not respond to the first order frequency of obliquity (41 kyr) between 1 and 2 Ma, the high variance at the 54-kyr cycle cannot be explained simply by orbital obliquity forcing. A dominant 54-kyr cycle also appears within the sedimentation rate record, which probably reduces or shifts the 41-kyr frequency in the dust flux spectrum.

The spectral evolution (Figure 9) implies that precessional low-latitude insolation forcing (the heating of land masses and modulation of the African monsoon) was the primary mechanism in controlling South Saharan and Sahelian aridity/humidity from 5 to 3 Ma. From 3 to 1.5 Ma, the AEJ dust flux responded to high-latitude insolation forcing associated with the size and boundary conditions of northern hemisphere ice sheets and to low-latitude forcing. During the last 1 m.y. the climatic evolution of the Sahel zone was primarily linked to high-latitude climate forcing associated with a repeated glacial expansion in northern hemisphere ice sheets at the 100-kyr rhythm.

Our interpretation of the spectral evolution of African climate agrees with *Bloemendahl and deMenocal* [1989] for the last 3.5 m.y. However, their magnetic susceptibility data (indicative of eolian sediment supply) did not note the long transitional interval from 3 to 1.5 Ma, where both precession and obliquity cycles are pronounced in the dust flux frequency spectrum.

Cross spectral phase relationships between the $\delta^{18}O$ and dust flux records at site 659 for ten succeeding time intervals (Fig. 11, Table 3) shows that during the last 5 m.y., dust flux maxima lead $\delta^{18}O$ maxima by 0.5-5 kyr at the main orbital frequencies of obliquity and precession, except for the obliquity related fluctuations between 3.5 and 4 Ma. However, this lag estimate (1.8 kyr) is based on low coherence just above the 80% confidence level and should be considered with great caution. The phase relationships indicate no significant evolutionary trend from 5 to 0.5 Ma and suggest no major change in the $\delta^{18}O$ response time to variations in high-latitude ice cover before and after the major phase of the Pliocene northern hemisphere ice growth. The phase differences between the $\delta^{18}O$ and dust flux records, however, reach a maximum during the last 0.5 m.y. at the periods of obliquity (4.9±1.5 kyr) and precession (3.6±0.6 kyr), which might be linked to changes in high-latitude climate boundary conditions, when the waxing and waning of polar ice sheets was dominated by the 100-kyr eccentricity cycle.

Further insights into the response times of the different dust transporting wind systems over northwest Africa with respect to climate forcing can be gained by comparing the records of northeast trade winter dust plume at equatorial site 663 [*deMenocal et al.*, 1993] with the SAL summer dust plume at site 659 (Figures 1 and 12). Both records are indicative of changes in South Saharan and Sahelian aridity. Over the last 0.5 m.y., the dust flux records at sites 659 and 663 exhibit a similar pattern of variation with maximum values during cold stages and minimum values during warm stages (Figure 12). However, the dust flux rates and the amplitude variations at site 659 exceed the variations at equatorial site 663 by a factor of 2 to 3.

The amount of dust transported into the Gulf of Guinea is mainly controlled by the latitudinal position of the ITCZ and the strength of the winter trades [*Ruddiman and Janecek*, 1989]. Today, most dust that is emitted from North Africa to the south is scavenged over the continent and/or at the moist ITCZ [*D'Almeida*, 1986], which reaches its southernmost position during boreal winter at 3°-5°N [*Tetzlaff and Peters*,

Table 3. Cross-spectral Phase Relationships and Cross Coherencies Between $\delta^{18}O$ (Reversed) and Dust Flux Records for Succeeding Time Intervals at Site 659 With Respect to Eccentricity (100 kyr), Obliquity (41 kyr) and Precession (23 and 19 kyr)

Time Interval (m.y.) of Cross Spectra $\delta^{18}O$ versus Dust Flux	Coherency and Phase			
	100 kyr	41 kyr	23 kyr	19 kyr
0 - 0.5	---	0.88 137±13	0.94 123±10	---
0.6 - 1	---	0.84 -189±17	---	0.95 104±8
1 - 1.5	0.75 88±22	---	0.92 -188±11	---
1.5 - 2	---	0.82 174±17	---	---
2 - 2.5	---	0.90 -197±12	0.88 -200±14	---
2.6 - 3	---	0.88 170±14	---	---
3 - 3.5	0.73 56±23	---	---	0.82 107±18
3.5 - 4	---	0.68 -165±26	0.81 -222±19	---
4 - 4.5	---	---	0.71 149±24	0.73 155±23
4.5 - 5	---	0.93 161±11	---	---

All relationships are coherent above the 80% confidence interval (nonzero coherency level = 0.64). For example, obliquity-related dust flux maxima lag $\delta^{18}O$ minima by 137° during the last 0.5 m.y. or dust flux maxima lead $\delta^{18}O$ maxima by 43° (see Figure 11).

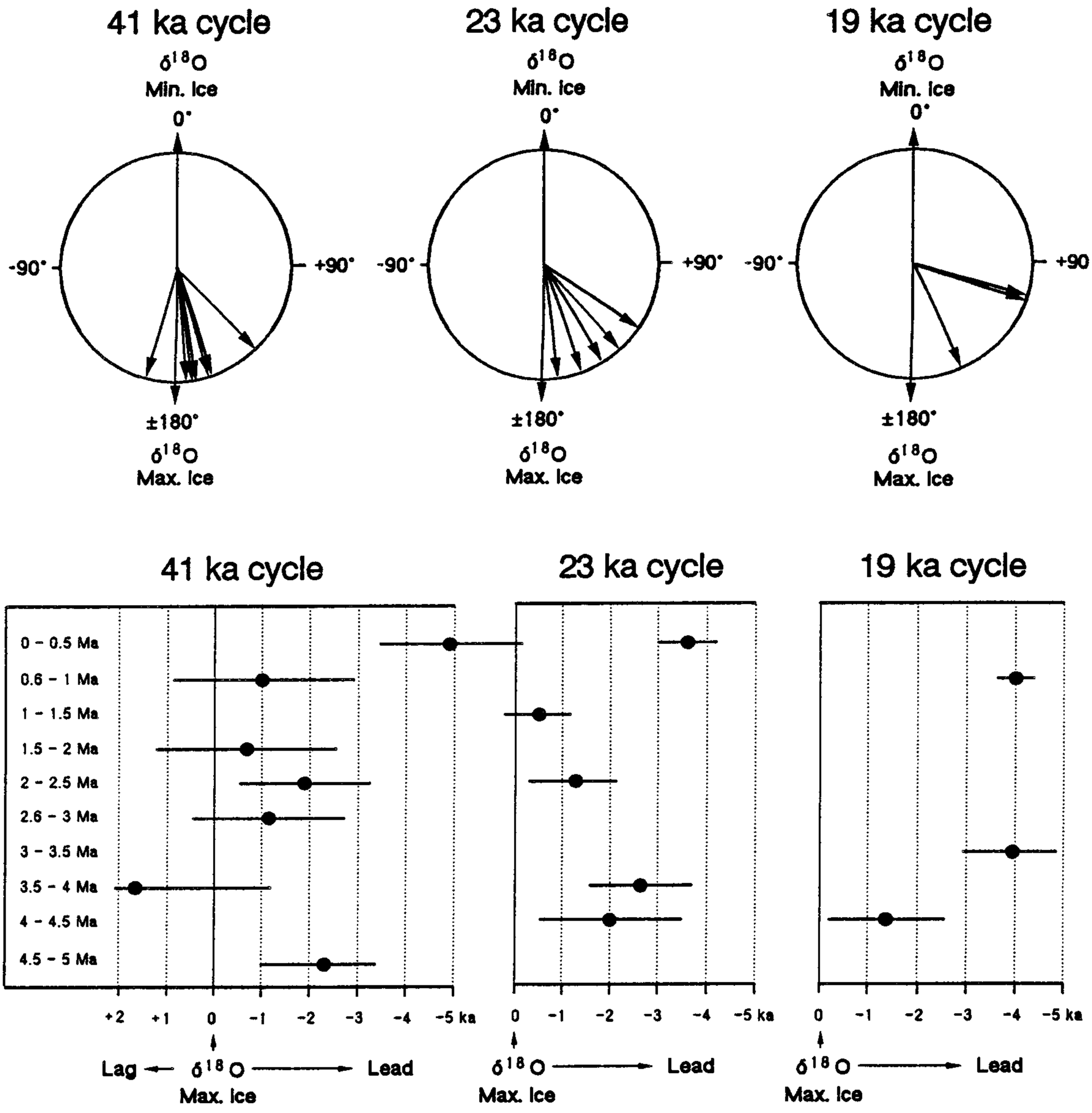

Figure 11. (top) Phase wheels for site 659 $\delta^{18}O$ and dust flux cycles at the obliquity (41 kyr) and precession (23 and 19 kyr) bands. Zero phase on each wheel is set at minimum $\delta^{18}O$. Dust flux vectors for preceeding time intervals between 0 and 5 Ma indicate the angular distance from 0° (minimum ice) or 180° (maximum ice). For example, dust flux maxima at the obliquity band lead $\delta^{18}O$ maxima by 3.6 kyr (32°/360°x 41 kyr) during the last 0.5 m.y. All phase angles are given in Table 3. (bottom) Leads and lags (in kiloyears) of dust flux maxima with respect to $\delta^{18}O$ maxima (max. ice) over the last 5 Ma at the obliquity and precession bands. Bars indicate error ranges.

1986]. Hence only minor dust is finally reaching the more southerly position of site 663 (1°S, 12°W).

An alternate way to check the correlation between the two dust records is to compare the response times of the SAL and northeast trade wind borne dust fluxes to global climate forcing. For the last 0.6 m.y., *deMenocal et al.* [1993] (see Table 3) estimated that the dust flux record led the planktonic $\delta^{18}O$ record by 61° (7 kyr) at the obliquity band. To be consistent with the estimates from site 659 (0-0.5 Ma), we recalculated the response times between the winter dust plume and the planktonic $\delta^{18}O$ record at site 663 using the same treatment for spectral analyses as applied to site 659. It turned out that the dust flux maxima at site 663 significantly ($k = 0.86$) lead the ice volume maxima by 51°±16° (5.8 kyr) at the obliquity band as compared to 43°±13° (4.9 kyr) at site 659 (Table 3). Hence the dust records at sites 659 and 663 are in phase within the error limits at the obliquity frequency band during the last 0.5 m.y. In contrast, the precessional frequencies at site 663 are incoherent and do not show any significant phase relationship.

In conclusion, the 41-kyr dust flux signals recorded at both sites appear sensitive to aridity and humidity in the dust source regions rather than to differences in the eolian transport dynamics (including dust generation) of the AEJ during

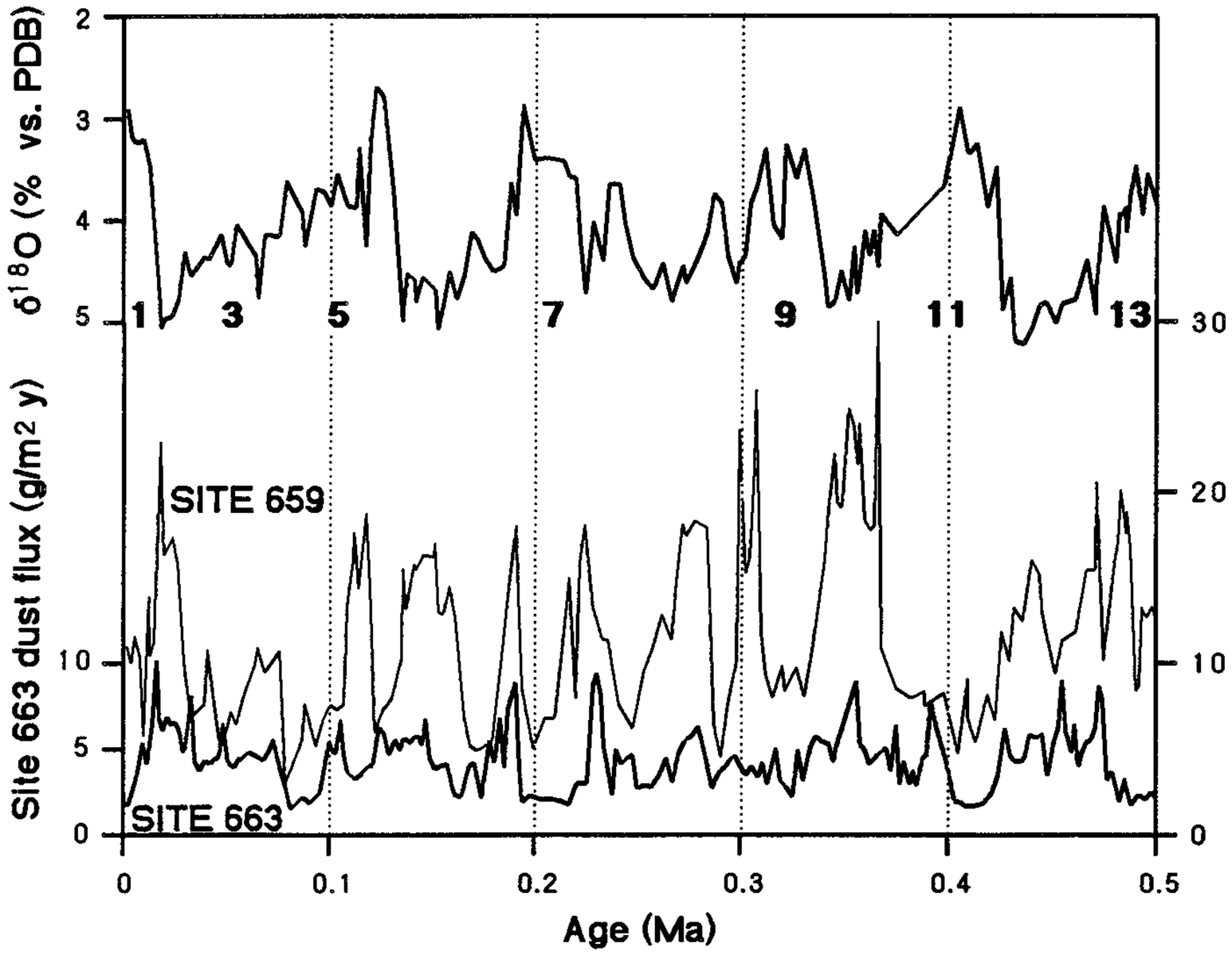

Figure 12. Dust flux records from sites 659 and 663 for the last 0.5 m.y. compared to the benthic $\delta^{18}O$ record (site 659).

summer and the winterly northeast trades. Differences, however, may occur in recording aridity changes linked to precessional forcing, because the frequency spectrum of the winter dust plume record indicates no significant power at the precessional bands, whereas the precessional spectrum of the SAL summer plume is well developed. An explanation for this discrepancy is that the variations in the dust discharge of trade winds are too weak to be recorded at the 23- to 19-kyr periodicities. Eolian grain size records may help to solve this problem.

Conclusions

We developed a new timescale for the Pliocene that extends the Atlantic oxygen isotope stratigraphy and numbering scheme of the isotope cycles from 2.85 back to 5 Ma. Our results suggest that the Pliocene dust flux record from site 659 can be calibrated accurately to the precessional component of the astronomical record (periods of 19 and 23 kyr). This tuning resulted in an independent calibration of the $\delta^{18}O$ record, which is marked by an increased concentration of variance at the obliquity cycle. The tuned ages for the magnetic reversal boundaries Gauss/Gibert and Top Cochiti are 6-7% older than conventional ages. This agrees with the conclusions of *Shackleton et al.* [1994b] and *Hilgen* [1991], implying that the Pliocene was about 500-kyr longer than previously assumed.

Dominant precession cycles in the dust flux record (site 659) indicate that the Pliocene climatic evolution of the South Sahara and Sahel zone was primarily linked to low-latitude monsoonal forcing from 3 to 4.5 Ma. A combined low-latitude and high-latitude climate forcing, indicated by dominant 19- to 23-kyr and 41-kyr dust flux cycles, occurred from 4.5 to 5 Ma and from 3 to 1.5 Ma. The Pleistocene dust flux cycles with high variance at the 100-kyr eccentricity period and at the obliquity related periods of 41-kyr and 54-kyr impling a dominant response to high-latitude climate forcing. From 5 to 0.5 Ma, the estimated time lags between the $\delta^{18}O$ and dust flux cycles indicate no evolutionary trend at the frequency bands of obliquity and precession. However, the time lags are significantly increased during the last 0.5 m.y., which might be linked to the evolution of the 100-kyr ice age cycles. Major long-term increases in the dust flux rates occurred from 2.8 to 2 Ma, parallel to a major phase of the northern hemisphere ice growth and near 1.6 to 1.4 Ma with the amplification of the Pleistocene ice age cycles.

The benthic oxygen isotope values (site 659) fluctuated mainly at the 41-kyr obliquity cycle over the last 5 m.y. No spectral variance at orbital frequencies occurred during the intervals from 4 to 4.5 Ma and 3 to 3.5 Ma, periods of low-amplitude variation in orbital obliquity.

An increasing number of deepwater incursions from the southern ocean during the late Pliocene glacial stages may have caused the enlarged $\delta^{18}O$ excursions at Atlantic site 659 as compared to the record of Pacific site 846.

Data

All data from ODP site 659 will be available from the first author (R.T.) on a 3.5 inch double density (double sided) 720 KB IBM-formatted disk. The ASCII files contain composite depth, age, oxygen isotope data from *C. wuellerstorfi* (corrected to seawater equilibrium), sedimentation rates, percentages of the siliciclastic fraction, dry bulk density values, and dust fluxes.

Acknowledgments. The authors are grateful to P. DeMenocal, L. Dupont, G. Haug, M.F. Loutre, U. Pflaumann, H. Schulz, F. Sirocko, and P. Weinholz for stimulating discussions and for suggestions in improving this study. K. Baumann (GEOMAR Kiel) kindly provided an unpublished extinction datum for *C. macintyrei*, and P. Cepek (Bundesanst. f. Geow. u. Rohst., Hannover) provided the first appearance datum of *C. rugosus*. U. Pflaumann kindly provided his unpublished computer software for spectral analysis. We gratefully acknowledge the cooperation with H. Erlenkeuser and H. Cordt, who supervised the operation of the mass spectrometer in Kiel with special care. C. Wold greatly assisted in improving the English of the manuscript. We thank S. Crowhurst, E. Heinrich, and J. Hennings for technical assistance. The Deutsche Forschungsgemeinschaft generously supported this study.

References

Backman, J., and N. J. Shackleton, Quantitative biochronology of Pliocene and early Pleistocene calcareous nannofossils from the Atlantic, Indian, and Pacific Oceans, *Mar. Micropaleontol., 8*, 141-170, 1983.

Baksi, A. K., V. Hsu, M. O. McWilliams, and E. Farrar, $^{40}Ar/^{39}Ar$ dating of the Brunhes-Matuyama geomagnetic field reversal, *Nature, 256*, 356-357, 1992.

Baksi, A. K., K. A. Hoffmann, and M. McWilliams, Testing the accuracy of the geomagnetic polarity time-scale (GPTS) at 2-5 Ma, utilizing $^{40}Ar/^{39}Ar$ incremental heating data on whole rock basalts, *Earth Planet. Sci. Lett., 118*, 135-144, 1993.

Berger, A., and M.F. Loutre, Insolation values for the climate of the last 10 million years, *Quat. Sci. Rev., 10*, 297-317, 1991.

Berggren, W. A., D. V. Kent, J. J. Flynn, and J. A. Van Couvering, Cenozoic geochronology, *Geol. Soc. Am. Bull., 96*, 1407-1418, 1985.

Bloemendahl, J., and P. deMenocal, Evidence for a change in the periodicity of tropical climate cycles at 2.4 Myr from whole-core magnetic susceptibility measurements, *Nature, 42*, 897-900, 1989.

Bloemendahl, J., L. Tauxe, and J.-P. Valet, High-resolution, whole-core magnetic susceptibility logs from leg 108, *Proc. Ocean Drill. Program Initial Rep. , 108*, 1005-1013, 1988.

Cande, S. C. and D. V. Kent, A new geomagnetic polarity timescale for the late Cretaceous and Cenozoic, *J. Geophys. Res., 97*, 13,917-13,951, 1992.

Chepstow-Lusty, A., J. Backman, and N. J. Shackleton, Comparison of upper Pliocene Discoaster abundance variations from North Atlantic sites 552, 607, 658, 659, and 662: Further evidence for marine plankton responding to orbital forcing, *Proc. Ocean Drill. Program Sci. Results, 108*, 121-141, 1989.

Curry, W. B. and G. P. Lohmann, Carbon deposition rates and deep water residence time in the equatorial Atlantic Ocean throughout the last 160,000 years, in *The Carbon Cycle and Atmospheric CO_2: Natural Variations Archean to Present, Geophys. Monogr. Ser.*, Vol. 32, edited by E.T. Sundquist and W.S. Broecker, pp. 223-350, AGU Washington, D.C., 1985.

D'Almeida, G. A., A model for Saharan dust transport, *J. Clim. Appl. Meteorol., 25*, 903-916, 1986.

deMenocal, P. B., W. F. Ruddiman, and E. M. Pokras, Influences of high- and low-latitude processes on African terrestrial climate: Pleistocene eolian records from equatorial Atlantic Ocean Drilling Program site 663, *Paleoceanography, 8*, 209-242, 1993.

Dhonneur, G., and Y. Tourre, Easterly waves and squall lines: two different phenomena, *Global Atmos. Res. Program, Special Rep., 37, App. 15*, pp. 9-15, Geneva, Switzerland, 1981.

Harrison, T. M., P. Copeland, W. S. F. Kidd, and A. Yin, Raising Tibet, *Science, 255*, 663-1670, 1992.

Hilgen, F. J., Extension of the astronomically calibrated (polarity) time scale to the Miocene/Pliocene boundary, *Earth Planet. Sci. Lett., 107*, 349-368, 1991.

Hills, S. J., and H. R. Thierstein, Plio-Pleistocene calcareous plankton biochronology, *Mar. Micropaleontol., 14*, 67-96, 1989.

Hooghiemstra, H., A. Bechler, and H. J. Beug, Isopollen maps for 18,000 years B.P. of the Atlantic offshore Northewest Africa: Evidence for paleowind circulation, *Paleoceanography, 2*, 561-582, 1987.

Imbrie, J., and J. Z. Imbrie, Modeling the climatic response to orbital variations, *Science, 207*, 943-953, 1980.

Imbrie, J., J. D. Hays, D. G. Martinson, A. McIntyre, A. C. Mix, J. J. Morley, N. G. Pisias, W. L. Prell, and N. J. Shackleton, The orbital theory of Pleistocene climate: Support from a revised chronology of the marine $\delta^{18}O$ record, in *Milankovitch and Climate*, edited by A. Berger and J. Imbrie, pp. 269-305, D. Riedel, Norwell, Mass., 1984.

Imbrie, J., E. A. Boyle, S. C. Clemens, A. Duffy, W. R. Howard, G. Kukla, J. Kutzbach, A. McIntyre, A. C. Mix, B. Molfino, J. J. Morley, L. C. Peterson, N. G. Pisias, W. L. Prell, M. E. Raymo, N. Y. Shackleton, and J. R. Toggweiler, On the structure and origin of major glaciation cycles, 1. Linear responses to Milankovitch forcing, *Paleoceanography, 7*, 701-738, 1992.

Imbrie, J., A. Berger, E. A. Boyle, S. C. Clemens, A. Duffy, W. R. Howard, G. Kukla, J. Kutzbach, D. G. Martinson, A. McIntyre, A. C. Mix, B. Molfino, J. J. Morley, L. C. Peterson, N. G. Pisias, W. L. Prell, M. E. Raymo, N. Y. Shackleton, and J. R. Toggweiler, On the structure and origin of major glaciation cycles: 2. The 100,000-year cycle, *Paleoceanography, 8*, 699-735, 1993.

Jansen, E., and J. Sjøholm, Reconstruction of glaciation over the past 6 Myr from ice-born deposits in the Norwegian Sea, *Nature, 349*, 600-603, 1991.

Jenkins, G. M., and D. G. Watts, *Spectral Analysis and Its Application*, 525 pp., Holden-Day, Oakland, Calif., 1968.

Kolla, V., P. E. Biscaye, and A. F. Hanley, Distribution of quartz in late Quaternary Atlantic sediments in relation to climate, *Quat. Res., 11*, 261-277, 1979.

Kutzbach, J. E., Monsoon climate of the early Holocene: climatic experiment using the earth's orbital parameter for 9,000 years ago, *Science, 214*, 59-61, 1981.

Kutzbach, J. E., and F. A. Street-Perrott, Milancovitch forcing of fluctuations in the level of tropical lakes from 18 to 0 kyr B.P., *Nature, 317*, 130-134, 1985.

Lamb, P. L., Large-scale tropical Atlantic surface circulation patterns associated with Subsaharan weather anomalies, *Tellus, 30*, 240-251, 1978.

Martinson, D. G., N. G. Pisias, J. D. Hays, J. Imbrie, T. C. Moore, and N. J. Shackleton, Age dating and the orbital theory of the ice ages: Development of a high-resolution O - 300,000-year chronostratigraphy, *Quat. Res., 27*, 1-29, 1987.

Mercier, J. L., R. Armijo, P. Tapponnier, E. Carey-Gailhrdis, and H. T. Lin, Change from late Tertiary compression to Quaternary extension in southern Tibet during the India-Asia collision, *Tectonics, 6*, 275-304, 1987.

Palmer, T. N., Influence of the Atlantic, Pacific and Indian Oceans on Sahel rainfall, *Nature, 322*, 251-253, 1986.

Parkin, D. W., and N. J. Shackleton, Trade wind and temperature correlations down a deep-sea core off the Sahara coast, *Nature, 245*, 455-457, 1973.

Pokras, E. M., and A. C. Mix, Eolian evidence for spatial variability of late Quaternary climates in tropical Africa, *Quat. Res., 24*, 137-149, 1985.

Prell, W. L., and J. E. Kutzbach, Monsoon variability over the past 150,000 years, *J. Geophys. Res., 82*, 8411-8425, 1987.

Quade, J., T. E. Cerling, and J. R. Bowman, Development of Asian monsoon revealed by marked ecological shift during the latest Miocene in northern Pakistan, *Nature, 342*, 163-165, 1989.

Raymo, M. E., W. F. Ruddiman, J. Backman, B. M. Clement, and D. G. Martinson, Late Pliocene variation in northern hemisphere ice sheets and North Atlantic deep water circulation, *Paleoceanography, 4*, 413-446, 1989.

Rea, D. K., and Leg 145 Scientific Shipboard Party, Paleoceanographic record of North Pacific quantified, *Eos. Trans., AGU, 74*(36), 406-411, 1993.

Rossignol-Strick, M., African monsoons, an immediate climate response to orbital insolation, *Nature, 304*, 46-49, 1983.

Ruddiman, W. F., et al., *Proc. Ocean Drill. Program Initial Rep., 108*, 1-1073, 1988.

Ruddiman, W. F., and T. R. Janecek, Pliocene-Pleistocene biogenic and terrigenous fluxes at equatorial Atlantic sites 662, 663, and 664, *Proc. Ocean Drill. Program Sci. Results, 108*, 211-240, 1989.

Ruddiman, W. F. and J. E. Kutzbach, Forcing of late Cenozoic northern hemisphere climate by plateau uplift in southern Asia and the American West, *J. Geophys. Res., 94*, 18,409-18,427, 1990.

Ruddiman, W. F., M. E. Raymo, and A. McIntyre, Matuyama 41,000-year cycles: North Atlantic Ocean and Northern Hemisphere ice sheets, *Earth Planet. Sci. Lett., 80*, 117-129, 1986.

Ruddiman, W. F., M. Samthein, J. Backmann, J. G. Baldauf, W. Curry, L. M. Dupont, T. Janecek, E. M. Pokras, M. E. Raymo, B. Stabell, R. Stein, and R. Tiedemann, Late Miocene to Pleistocene evolution of climate in Africa and the low latitude Atlantic: Overview of leg 108 results. *Proc. Ocean Drill. Program Sci. Results, 108*, 463-484, 1989

Samthein, M., and R. Tiedemann, Toward a high-resolution stable isotope stratigraphy of the last 3.4 million years: Sites 658 and 659 off northwest Africa, *Proc. Ocean Drill. Program Sci. Results, 108*, 167-185, 1989.

Samthein, M., G. Tetzlaff, G. Koopmann, K. Wolter, and U. Pflaumann, Glacial and interglacial wind regimes over the eastern sub-tropical Atlantic and northwest Africa, *Nature, 293*, 193-196, 1981.

Samthein, M., J. Thiede, U. Pflaumann, H. Erlenkeuser, D. Fütterer, B. Koopmann, H. Lange, and E. Seibold, Atmospheric and oceanic circulation patterns off northwest Africa during the past 25 million years, in *Geology of the Northwest African Continental Margin*, edited by U. von Rad, M. Samthein, and E. Seibold, pp. 584-604, Springer-Verlag, New York, 1982.

Schulz, H., Hochauflösende Sauerstoff- und Kohlenstoff-isotopenstratigraphie im frühen Pliozän vor 3.4 bis 4.6 Millionen Jahren: ODP Site 659, Subtropischer Ostatlantik, Masters thesis, 34pp., Univ. Kiel, Hiel, Germany, 1988.

Shackleton, N. J., and M. A. Hall, Oxygen and carbon isotope stratigraphy of Deep Sea Drilling Project hole 552A: Plio-Pleistocene glacial history, *Initial Rep. Deep Sea Drill. Proj., 81*, 599-609, 1984.

Shackleton, N. J., A. Berger, and W. R. Peltier, An alternative astronomical calibration of the lower Pleistocene timescale based on ODP site 677, *Trans. R. Soc. Edinburgh Earth Sci., 81*, 251-261, 1990.

Shackleton, N. J., M. A. Hall, and D. Pate, Pliocene stable isotope stratigraphy of ODP site 846, *Proc. Ocean Drill. Program Sci. Results*, in press, 1994a.

Shackleton, N. J., S. Crowhurst, T. Hagelberg, N. G. Pisias, and D. A. Schneider, A new late Neogene time scale: Application to leg 138 sites, *Proc. Ocean Drill. Program Sci. Results*, in press, 1994b.

Stein, R., Late Neogene evolution of paleoclimate and paleoceanic circulation in the northern and southern hemispheres - A comparison, *Geol. Rundsch., 75*, 125-138, 1986.

Stein, R., H. L. ten Haven, R. Littke, J. Rullkötter, and D. H. Welte, Accumulation of marine and terrigenous organic carbon at upwelling site 658 and nonupwelling sites 657 and 659: Implications for the reconstruction of paleoenvironments in the eastern subtropical Atlantic through late Cenozoic times, *Proc. Ocean Drill. Program Sci. Results, 108*, 361-386, 1989.

Street, F. A., and A. T. Grove, Global maps of lake-level fluctuations since 30,000 yr B.P., *Quat. Res., 12*, 83-118, 1979.

Street-Perrott, F. A., and R. A. Perrott, Abrupt climate fluctuations in the tropics: The influence of Atlantic Ocean circulation, *Nature, 343*, 607-612, 1990.

Tauxe, L., A. D. Deino, A. K. Behrensmeyer, and R. Potts, Pinning down the Brunhes/Matuyama and upper Jaramillo boundaries: A reconcilation of orbital and isotope time scales, *Earth Planet. Sci. Lett., 109*, 561-572, 1992.

Tetzlaff, G., and M. Peters, The atmospheric transport for water vapor and dust in the Sahel region, *Geol. J., 12*, 387-398, 1986.

Tiedemann, R., Acht Millionen Jahre Klimageschichte von Nordwest Afrika und Paläozeanographie des angrenzenden Atlantiks: Hochaufösende Zeitreihen von ODP-Sites 658-661, *Ber. 46*, 190pp., Geol.-Paläont. Inst. Univ. Kiel, Kiel, Germany, 1991.

Tiedemann, R., M. Samthein, and R. Stein, Climatic changes in the western Sahara: Aeolo-marine sediment record of the last 8 million years, *Proc. Ocean Drill. Program Sci. Results, 108*, 241-278, 1989.

Walter, R. C., P. C. Manega, R. L. Hay, R. E. Drake, and G. H. Curtis, Laser-fusion $^{40}Ar/^{39}Ar$ dating of bed I, Olduvai George, Tanzania, *Nature, 354*, 145-149, 1991.

Weaver, P. P. E., et al., Biostratigraphic synthesis, leg 108, eastern equatorial Atlantic, *Proc. Ocean Drill. Program Sci. Results, 108*, 455-462, 1989.

Zahn, R., K. Winn, and M. Samthein, Benthic foraminiferal $\delta^{13}O$ and accumulation rates of organic carbon: *Uvigerina peregrina* group and *Cibicidoides wuellerstorfi*, *Paleoceanography, 1*, 27-42, 1986.

M. Samthein, Geologisch-Paläontologisches Institut, Universität Kiel, Olshausenstraße 40, D-24098 Kiel, Germany.

N. J. Shackleton, Godwin Laboratory, University of Cambridge, Free School Lane, Cambridge, CB 3RS, England.

R. Tiedemann, GEOMAR, Forschungszentrum für marine Geowissenschaften, Universität Kiel, Wischhofstr. 1-3, D-24148 Kiel, Germany.

(Received June 7, 1993; revised January 10, 1993;
accepted January 17, 1993)